Julia Zinsmeister, Michael Storch1, Jens Melder, Sandra Richter, Nina Gaiser, Samuel Schlichting, Clemens Naumann, Erik Schünemann1, Manfred Aigner, Patrick Oßwald, Markus Köhler, Soot Formation of renewable gasoline: From fuel chemistry to particulate emissions from engines, Fuel 348 (2023) 128109
1 Robert Bosch GmbH, Powertrain Solutions, Renningen, Germany

The original publication is available at www.elsevier.com

https://doi.org/10.1016/j.fuel.2023.128109/

Soot formation of renewable gasoline: From fuel chemistry to particulate emissions from engines

Julia Zinsmeister[a*], Michael Storch[b], Jens Melder[a], Sandra Richter[a], Nina Gaiser[a], Samuel Schlichting[a], Clemens Naumann[a], Erik Schünemann[b], Manfred Aigner[a], Patrick Oßwald[a], Markus Köhler[a]

[a] *German Aerospace Center (DLR), Institute of Combustion Technology, Pfaffenwaldring 38-40, 70569 Stuttgart, Germany*

[b] *Robert Bosch GmbH, Powertrain Solutions, Robert-Bosch-Campus 1, 71272 Renningen, Germany*

* Corresponding author: Julia Zinsmeister,
German Aerospace Center, Pfaffenwaldring 38-40, 70569 Stuttgart, Germany
Phone: +49-711-6862-8143; Email: Julia.Zinsmeister@dlr.de

Abstract

Renewable fuels are essential to meet climate protection goals, especially for decarbonizing the existing vehicle fleet. In addition, optimized and specially designed fuels allow emissions to be avoided before they occur. This paper presents fuel effects on emission characteristics of six chemically complex gasoline blends compliant with the DIN EN 228 standard and one ethanol/gasoline blend, focusing on particle emissions. First, the sooting propensity of the fuels was examined using different soot indices, such as the Particulate Matter Index (PMI), the Oxygen Extended Sooting Index (OESI), the Yield Sooting Index (YSI), and the soot threshold (φ_{ST}), which is drawn on measurements of the particle number (PN) density in the exhaust gas of a laminar flat flame. Second, PN emissions (particle number concentration) from a production-calibrated turbo gasoline direct injection engine with four cylinders were investigated. Third, soot precursor chemistry was investigated using a laminar flow reactor at atmospheric pressure. Finally, correlations to fuels' volatility and chemical characteristics were made for the complete data set. Based on the soot precursor chemistry in the homogeneous gas phase reaction, it was found that engine PN emissions are primarily influenced by fuel chemistry for the investigated engine conditions. In particular, the composition of the hydrocarbon fraction is decisive, with the heavy

C9+ aromatics and the upper distillate significantly influencing soot formation. Future fuels should contain fewer soot-increasing hydrocarbon fractions to reduce PN engine emissions.

Keywords

Drop-in renewable fuels, Alternative gasoline, Engine emissions, Particle number (PN), Sooting tendency indices, Soot precursor chemistry

1. Introduction

With the "Fit for 55" legislative package, the European Commission proposed a revision of almost all relevant policy instruments to achieve the new EU climate target: Reduce the amount of greenhouse gas (GHG) emissions emitted by at least 55 percent below the 1990 level (55 % target). The transport sector accounts for about one-third of the final energy consumption within the EU. The required energy is predominantly provided by fossil fuels, making transport responsible for a large share of GHG emissions [1]. Since 2009, the EU has been limiting the CO_2 emissions of new cars and vans, and since 2020 also of trucks and buses. To reach the EU greenhouse gas reduction targets in this sector, the market penetration of battery electric vehicles powered with CO_2-neutral electricity and the introduction of vehicles powered with CO_2-neutral hydrogen is significant. Although the number of new registered electric vehicles in the EU is growing steadily, more than 75 % of the legacy vehicle fleet in 2020 still operated with combustion engines (diesel and gasoline) [2]. However, the existing vehicle fleet is not mentioned in climate plans despite the remaining high number of vehicles with combustion engines in 2030 and beyond.

The only way to address the existing vehicle fleet, including the corresponding infrastructure, is by introducing renewable fuels that comply with current fuel standards, like DIN EN 228 for gasoline specification in the EU. Such an alternative renewable fuel can be denoted as a drop-in renewable fuel. Hartung et al. [3] proposed, within a well-to-wheel study, that in 2030 the CO_2 emissions target of the European road traffic sector will be failed, although pure electrification of the sector was assumed. With the introduction of alternative renewable fuels, the difference between proposed CO_2 emission and GHG target can be reduced, but a gap will remain. The study showed that with a significant increase in renewable fuel production, the CO_2 target can be met and even exceeded by 2040.

The usability of renewable fuels in the legacy fleet and fuel distribution infrastructure is associated with the compliance of renewable fuels with current fuel standards. These drop-in fuels, including 2nd generation biofuels and e-fuels, can consist of renewable components blended into conventional gasoline and diesel base fuel. Today, it is already feasible to produce and utilize up to 100 % drop-in renewable fuels with favorable properties [4-6]. This allows for a flexible ramp-up of the renewable content, which can be adjusted according to the accessibility of renewable feedstock and the availability of drop-in renewable fuels in the respective markets.

A dynamic test bench study with a modern gasoline direct injection engine has shown that gaseous pollutant emissions (NO_x, HC, CO) of different DIN EN 228 compliant fuels, including renewable candidates are similar and less affected by fuel parameters, renewable content, operating condition (20 °C and -7 °C), and the characteristic test cycle (WLTC and RDE) [7]. This and other renewable fuel studies [8] have shown that engine out particle number (PN) emissions can vary more significantly depending on fuel parameters.

With the rollout of the new EU6d exhaust emission standard, vehicles are equipped with advanced emission reduction technologies and noticeable air quality improvements can be achieved with the planned entry into force of the EU7 standard in 2025, a further tightening of vehicle emission limits is expected. PN emissions are reduced by applying particulate gasoline filters (GPF) and are likewise included. Note that legacy vehicles may not be equipped with a GPF. Since this study focuses on renewable drop-in fuels designed for DIN EN 228 and the legacy vehicle fleet, PN emissions should mainly be evaluated for new fuel candidates.

The formation of soot particles already begins in the homogeneous gas phase, with soot precursor species, which is shown in Fig. 1. The well-accepted overall picture of soot formation in hydrocarbon flames is that small aromatics like benzene (C_6H_6) and toluene (C_7H_8) up to high-molecular-weight polycyclic aromatic hydrocarbons (PAHs) such as fluorene ($C_{13}H_{10}$) and phenanthrene ($C_{14}H_{10}$) are formed by smaller unsaturated hydrocarbon species, such as acetylene, ethene, propene, allene, propyne, and cyclopentadiene. Resonance-stabilized hydrocarbon radicals such as propargyl and allyl are also involved in the formation process of the aromatic ring structure [9-13]. In addition, the aromatics already contained in the fuel act directly as aromatic soot precursors. Polymerization reactions of the aromatic

97 species form higher PAHs with increasing size. Nucleation and surface growth leads to the formation of
98 primary particles, which subsequently may agglomerate to finally form visible soot [14].

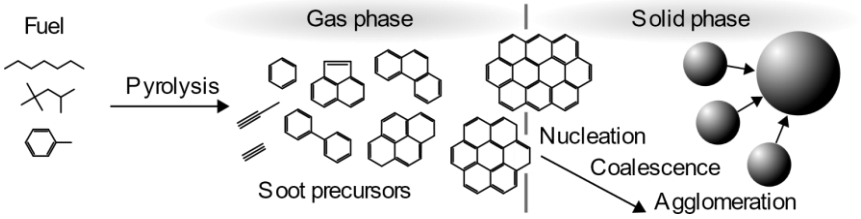

Fig. 1. Principle schema of soot particle formation. Adapted from [15].

99 Research into soot formation during the combustion of technical fuels, i.e. a chemically complex mixture
100 of numerous substances, which also include most alternative gasoline blends, has so far focused firmly
101 on engine experiments, e.g., [6-8] and evaluation of fuel sooting propensity using various soot indices,
102 such as Particulate Matter Index (PMI) [16], Threshold Soot Index (TSI) [17], Oxygen Extended Sooting
103 Index (OESI) [18], and Yield Sooting Index (YSI) [19, 20]. (For detailed information see chapter 3).
104 For chemical-kinetic model development, the complex fuels are simplified to surrogates consisting of
105 only a few components. Thus, experimental investigation of combustion chemistry also focuses on the
106 analysis of single- and multi-component systems, such as Primary Reference Fuels (PRFs), which are a
107 mixture of *n*-heptane and isooctane (2,2,4-trimethylpentane) and more often extended with toluene
108 (TPRFs), e.g., [21-23]. In addition, Fuels for Advanced Combustion Engines (FACE) types of gasoline,
109 which were developed based on statistical methods, to tackle properties of primary importance to engine
110 performance (anti-knock, aromatics, and normal-paraffin content) [24], have been widely studied, e.g.,
111 [22, 25]. However, detailed speciation data on the oxidation of real technical gasoline fuels are seldom
112 reported in the literature. Qi and coworkers [26, 27] studied lean and rich premixed flames fueled with
113 standard unblended gasoline with tunable synchrotron vacuum UV photoionization and identified more
114 than eighty intermediates, including oxygenated compounds and PAHs. More recently, Wang's research
115 group [28] presented results for two gasoline fuels and applied the HyChem approach to developing
116 reaction models for those real fuels.

117 This study investigates fuel effects on emission characteristics of six technical gasoline blends compliant
118 with DIN EN 228 and one ethanol/gasoline blend. The focus lies on soot formation. First, the sooting
119 propensity is examined by the use of different soot indices, such as PMI, OESI, YSI, and the premixed

flat flame-based soot threshold (φ_{ST}). Then, the PN emissions from a near-production calibrated turbo gasoline direct injection engine with four cylinders are determined. The particle formation is traced to its origin in the gas phase using an atmospheric laminar flow reactor system to study the soot precursor chemistry. Correlations between engine emissions and soot precursors are made to fuels' volatility and chemical characteristics, and finally, the data sets are compared.

2. Fuel characteristics

The following chapter introduces the set of fuels investigated in this study. The fuels are discussed alongside with their properties with a focus on their sooting behaviour.

2.1 Investigated fuels

The test fuels in this study include a set of six chemically complex gasoline blends that comply with the European standard DIN EN 228 and can thus be considered drop-in renewable fuels. Each of the fuels is designed to maximize the individual content of sustainable compounds, that may be produced on an industrial scale using available technologies. Considered compounds are methyl-*tert*-butyl ether (MTBE), ethyl-*tert*-butyl ether (ETBE), isobutanol (iBuOH; 2-methyl-1-propanol), and a Fischer-Tropsch (FT) product. The set, therefore, represents an option for immediate reduction of the CO_2 footprint and can directly be applied using the present technology and infrastructure. A summary of the fuels and their properties is listed in Table 1. Each component exploited the DIN EN 228 limits in this study, resulting in MTBEmax, ETBEmax, and iBuOHmax fuels. These oxygenates are primarily limited by the upper limit of oxygen mass fraction. A Fischer-Tropsch (FT) model fuel (so-called surrogate) was used to increase the proportion of renewable components. In a blend with 22 %(v/v) MTBE, 18 %(v/v) FT-Surrogate could be added, resulting in FT(18)MTBE fuel and in a blend with 20 %(v/v) ETBE, 20 %(v/v) FT-Surrogate could be added, resulting in FT(20)ETBE fuel. Finally, isooctane was added to an ETBE/FT-Surrogate/gasoline blend to increase the renewable component proportion even more. Hence, with a volumetric proportion of 23 % isooctane, a renewable energy content of 63 % was reached, still in compliance with DIN EN 228. This renewable fuel candidate is named ReMax. The fuel series is extended by an ethanol/gasoline blend, which contains a volumetric proportion of 30 % ethanol and is not compliant with DIN EN 228, named E30 [29]. The potential fuel candidates are compared to a fossil reference fuel (RefEU5Cert). RefEU5Cert contains a high aromatics content and poor boiling

148 behavior concerning the European fuel market. This fuel can be considered a bad case of European
149 market fuel concerning particulate emissions. The renewable fuel candidates MTBEmax, ETBEmax,
150 iBuOHmax, FT(18)MTBE, and FT(20)ETBE were designed to have similar aromatics content and
151 boiling behavior as the RefEU5Cert fuel. In summary, the fuel section reflects the maximized amount
152 of renewable content for the respective candidates currently under discussion while still being allowed
153 to be applied in current engine technology.

154 Fuel characterization, including the elemental composition (C/H/O), the detailed chemical composition
155 by hydrocarbon classes and oxygenates, as well as the sooting tendency utilizing smoke point (SP)
156 measurements, has been described in ref [30]. In this work, we have extended the set of fuel properties
157 to include volatility characteristics such as distillation data, vapor pressure, and enthalpy of vaporization
158 (ΔH_{vap}). The individual aromatic classes, broken down by their C-atom number, are included as well as
159 different soot indices (PMI, OESI, YSI, and φ_{ST}). Fundamental fuel properties are summarized in
160 Table 1, and the underlying methodologies are individually described in the following chapters. An
161 extended summary of fuels' properties can be found in table S1.
162

Table 1
Summary of fuels' fundamental properties.

	RefEU5 Cert	MTBE max	ETBE max	iBuOH max	FT(18) MTBE	FT(20) ETBE	ReMax	E30
RON (-) [a]	96.1	98.0	98.3	98.8	97.5	97.4	98.0	103.3
Density @15 °C (kg/m³) [b]	748.5	759.7	756.8	757.7	766.5	767.5	732.3	745.7
DVPE @37.8 °C (kPa) [c]	59.9	58.5	58.8	58.1	59.0	55.3	57.6	101.9
Distillation								
E150 (%(v/v)) [d]	83.2	78.2	79.9	82.3	82.3	81.9	88.4	92.8
IBP (°C) [d]	33.4	32.9	30.5	30.3	30.6	32.8	33.2	25.2
T70 (°C) [d]	116.5	131.6	121.7	110.6	118.6	114.3	101.3	78.1
T80 (°C) [d]	135.8	154.0	150.1	142.5	140.6	141.6	112.4	122.9
T90 (°C) [d]	175.3	177.0	173.7	171.0	176.1	176.9	171.9	143.0
FBP (°C) [d]	200.5	197.9	197.3	195.1	196.2	196.2	197.4	199.6
ΔH_{vap} mol (kJ/mol) [e]	27.6	25.4	25.0	25.6	25.0	24.7	25.2	24.9
ΔH_{vap} spec (kJ/kg) [f]	272.9	257.7	247.6	272.4	257.2	245.7	244.5	308.7
Detailed hydrocarbons + oxygenates analysis (GCxGC)								
n-Paraffins (%(m/m)) [g]	11.20	9.89	13.19	4.93	12.29	13.58	10.89	5.37
Isoparaffins (%(m/m)) [g]	32.86	19.73	11.83	28.07	12.30	10.02	35.80	25.69
Olefins (%(m/m)) [g]	6.45	5.90	6.82	5.56	6.83	5.99	3.67	14.10
Naphthenes (%(m/m)) [g]	3.35	5.76	5.99	8.68	9.20	11.33	11.41	2.22
Aromatics (%(m/m)) [g]	40.76	38.94	38.73	35.47	38.10	36.29	14.65	22.27
C7 Aromatics (%(m/m)) [g]	14.77	6.91	7.31	8.34	14.06	12.13	0.13	2.16
C8 Aromatics (%(m/m)) [g]	3.11	8.61	9.53	8.19	3.91	2.49	0.17	19.10
C9 Aromatics (%(m/m)) [g]	9.04	8.75	8.26	7.67	7.57	8.83	2.05	0.73
C9+ Aromatics (%(m/m)) [g]	22.88	23.17	21.67	18.73	20.12	21.67	14.35	0.97
Molar weight (g/mol) [h]	100.15	98.92	101.25	93.76	97.12	100.91	103.44	80.71
#C (mol) [i]	7.08	6.86	7.02	6.46	6.73	7.01	7.05	5.10
#H (mol) [i]	13.11	12.82	13.01	12.35	12.40	12.96	14.77	10.87
#O (mol) [i]	0.12	0.22	0.24	0.23	0.24	0.23	0.24	0.53
H/C molar (-) [j]	1.85	1.87	1.85	1.91	1.84	1.85	2.10	2.13
IHD (-) [k]	1.53	1.46	1.52	1.29	1.53	1.53	0.66	0.66
PMI (-) [l]	2.20	2.34	2.19	2.04	2.27	2.11	1.69	0.82
OESI (-) [m]	25.6	23.7	25.3	21.0	23.0	22.3	15.2	8.5
YSI (-) [n]	122.70	117.43	118.40	102.79	111.30	114.42	82.32	58.87
φ_{ST} (-) [o]	1.65	n.a.	1.70	1.70	n.a.	1.76	1.81	1.83

[a] Research Octane Number (RON), according to ASTM D2699, Source: Coryton, England [31].
[b] Density (ρ) measured according to EN ISO 12185. Ref [30].
[c] Dry Vapor Pressure Equivalent (DVPE) at 37.8°C, according to EN 13016-1, Source: Coryton, England [31].
[d] Distillation data, according to ASTM D86, Source: Coryton, England [31].
[e] Molar enthalpy of vaporization (ΔH_{vap}), calculated from vapor pressure measurements.
[f] Specific enthalpy of vaporization (ΔH_{vap}), calculated from vapor pressure measurements and molar weight.
[g] Detailed hydrocarbon + oxygenates analysis measured by two-dimensional gas chromatography (GCxGC). Ref [30].
[h] Molecular weight (MW) calculated from two-dimensional gas chromatography (GCxGC). Ref [30].
[i] Average sum formula calculated from two-dimensional gas chromatography (GCxGC).
[j] Molar Hydrogen to Carbon ratio (H/C) calculated from two-dimensional gas chromatography (GCxGC).
[k] Index of Hydrogen Deficiency (IHD) calculated from two-dimensional gas chromatography (GCxGC) acc. to Eq. (1).
[l] Particulate Matter Index (PMI) calculated according to Eq. (2). Source: Coryton, England [31].
[m] Oxygenate Extended Sooting Index (OESI) calculated from SP measurements according to Eq. (3).
[n] Yield Sooting Index (YSI) calculated from two-dimensional gas chromatography (GCxGC) according to Eq. (5).
[o] Soot threshold (φ_{ST}) determined from measurements conducted according to methods and materials chapter 3.1.

163

164 *2.2 Chemical characteristics*

165 It is known that unsaturated compounds tend to form more soot than paraffinic compounds. The sooting
166 tendency follows the sequence: paraffins < olefins < naphthenes < mono-aromatics < poly-aromatics
167 [17]. The unsaturation of a hydrocarbon compound can be understood as the lack of hydrogen, which
168 can be captured by the index of hydrogen deficiency (IHD) also called degree of unsaturation (DU) or
169 double bond equivalent (DBE), and is long-known [32, 33]. For a fuel containing the elements carbon,
170 hydrogen, and oxygen with an average formula $C_nH_mO_p$ the index of hydrogen is calculated as:

$$\mathrm{IHD} = (\mathrm{n}+1) - \left(\frac{m}{2}\right) = MW_{Fuel}\left(\frac{w_C}{MW_c} - \frac{w_H}{2 * MW_H}\right) + 1 \quad (1)$$

171 Where n, m, and p are the number of carbon, hydrogen, and oxygen atoms, respectively. MW is the
172 molar weight, and w is the weight proportion, where the subscript C stands for carbon and H for
173 hydrogen. The average molar weight of the fuel MW_{Fuel} can be calculated from a detailed chemical
174 composition analysis.

175 As could be seen in Eq. (1), isomeric structures, such as chain branching, are not distinguished.
176 Furthermore, the IHD counts the C=O double bond of carbonyl groups equally to carbon-carbon and
177 aromatic double bonds. However, carbonyl compounds are not a significant constituent of the present
178 fuels. Consequently, IHD is not directly influenced by the number of oxygen atoms. Both factors, the
179 fuels' molecular structure and the oxygen bound in the molecule, significantly affect the sooting
180 tendency of fuel [34-36]. IHD is closely linked to the molar hydrogen to carbon ratio (H/C) and has
181 proven its ability as an indicator affecting fuels' sooting tendency and particulate engine emissions for
182 hydrocarbon fuels. However, it is well known that introducing oxygen to the molecular structure
183 decreases the sooting propensity of a fuel, while C-C double bonds lead to an increase [37]. For this
184 reason, applying the IHD (or H/C) without further consideration of the molecular-bounded oxygen needs
185 to fail when the fuels to be compared deviate significantly in the oxygen content or the respective
186 molecular structure of the oxygenate. However, within the presented fuel series, a certain correlation
187 between sooting behavior and IHD is present due to their similar oxygen content.

188 As stated before, aromatics are more prone to form soot than saturated hydrocarbons, which is why
189 special attention was given to fuels' aromatics content in research to particulate engine emissions, e.g.,

[38-43], as well as in fundamental combustion research, e.g., [19, 30, 44]. Especially heavy, high molecular weight aromatics with carbon chain lengths equal to and greater than nine atoms (C9+ aromatics) are particularly interesting.

Composition of the investigated fuels. For all investigated fuels the detailed chemical composition was determined using two-dimensional gas chromatography (GCxGC) [30]. The technique allows for proper separation and classification of all fuel constituents by coupling two chromatographic separations with different polarities. In Fig. 2, results by group (paraffins, olefins, naphthenes, and aromatics) of the detailed chemical composition are given in comparison to the data set of 280 conventional summer-grade gasoline fuels [45] (box-plots). Considering the sum groups, all test fuels are in the same range as the comparison data set. A look at the individual aromatic classes, broken down by their C-atom number, reveals a fuel composition that differs noticeably from the conventional gasoline data set. On the one hand, the investigated standard-compliant gasoline blends have fewer C8 aromatics than the comparative data set's average. On the other hand, they exhibit a significantly higher proportion of C10 aromatics. This is different for the E30, which has increased C8 aromatics, but almost no C9+ aromatics. This fuel set can thus be used to specifically investigate the influence of heavy, high molecular weight aromatics with carbon chain length equal to and greater than 9 (C9+ aromatics) on emission characteristics of gasoline.

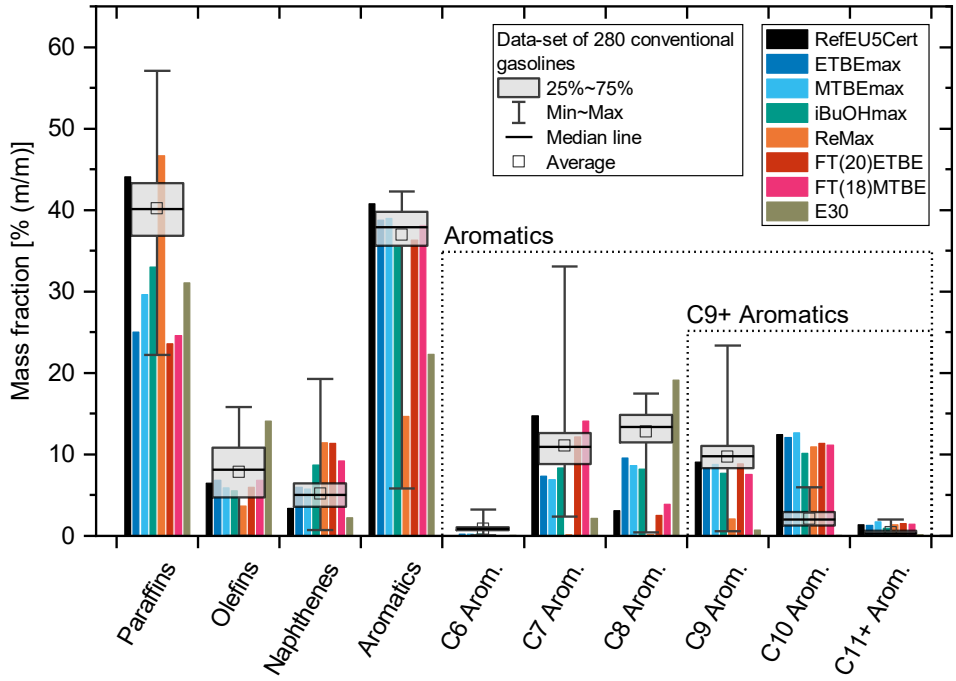

Fig. 2. Hydrocarbon groups of the investigated gasoline blends in comparison to the reference data of 280 conventional types of gasoline [45].

2.3 Volatility

Distillation data could characterize fuel's volatility. Measurements are performed according to the EN ISO 3405 standard. Unlike pure substances, mixtures of different compounds do not have a single value as their boiling point, but their evaporation occurs within a temperature range (= boiling range). The boiling curves indicate the evaporation temperature at which a certain volume fraction of the liquid mixture is evaporated. The initial boiling point (IBP) corresponds to the boiling point of the lightest component, and the final boiling point (FBP) corresponds to the heaviest component's boiling point. In particular, the volume fraction evaporated at 70 °C, 100 °C, and 150 °C (E70, E100, E150) and the FBP are essential volatility requirements for the use of gasoline on the European market (DIN EN 228). E70 represents the lower boiling end, E100 captures the middle distillate volatility, and E150 is the upper boiling end. Vapor pressure can also be regarded as a characteristic value for fuel volatility. In DIN EN 228, the Dry Vapor Pressure Equivalent (DVPE) measured at 37.8 °C (100 °F) according to EN 13016-1 is specified. Particular interest in studies of particulate emissions from engines is given to the upper boiling end, which includes the T70/780/T90/T95 points, e.g., [38, 43].

Volatility characteristics of the investigated fuels. In Fig. 3, the distillation profiles measured according to ASTM D86 standard test method (by Coryton, England [31]) are shown and compared to the data set of 280 different conventional types of gasoline [45] (solid lines forming a grey area) and three ethanol/gasoline blends (dashed lines). Two distillation curves particularly stand out. One is the ethanol/gasoline blend E30, which shows a flat section just above E70 (75 – 79 °C) corresponding to the boiling point of ethanol (78.3 °C). This is similar to the other three ethanol/gasoline blends. Secondly, the blend ReMax, where a large more volume fraction is evaporated at E100 than for the other standard-compliant test fuels. This can be attributed to the high isooctane proportion (boiling point 99 °C). The high C9+ aromatics content of the test fuels is reflected in the upper end of the distillation curves, resulting in higher T80/T85/T90 values compared to the 280 gasoline data set [45]. The final boiling point (FBP) of all fuel candidates is similar.

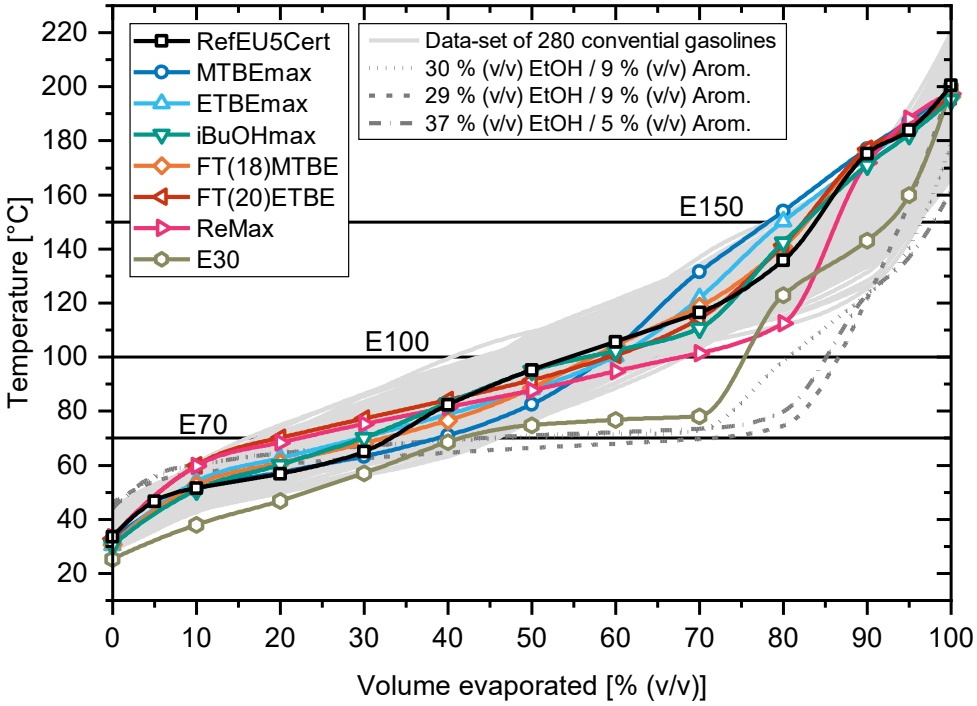

Fig. 3. Distillation curves in comparison to reference data of 280 conventional types of gasoline [45] (Lines = Akima Splines).

Considering Dry Vapor Pressure Equivalent (DVPE) measured at 37.8 °C (100 °F), the ethanol/gasoline blend E30 is the most volatile fuel candidate and has a DVPE almost twice as high as the standard-compliant fuels. In addition to DVPE, vapor pressure curves over a temperature range of 0 – 70 °C were measured according to ASTM D6378 and can be taken from the supplemental material.

To gain an impression of the evaporation behavior of the different fuel blends, the enthalpy of vaporization (ΔH_{vap}) was approximated from measured vapor pressure curves using the Clausius-Clapeyron equation. The Clausius-Clapeyron equation suggests that a plot of ln(p) vs. T^{-1} should yield a straight line, with the slope equal to $-\Delta H_{vap}/R$. It is assumed that ΔH_{vap} is constant over the range of temperature. This rather rudimentary approach was already used earlier to approximate ΔH_{vap} for gasoline [46, 47]. Note that this method is initially used for pure components, while the ideal gas state is assumed, and thus it is only a rough estimation of ΔH_{vap} for complex fuel mixtures. Especially for ethanol/gasoline blends, ΔH_{vap} results may contain a significant error due to the high ΔH_{vap} of ethanol ($\Delta H_{vap,ethanol}$@25 °C: ~ 918 kJ/kg [48]) compared to gasoline hydrocarbon components ($\Delta H_{vap,gasoline\text{-}CH}$: 350 to 400 kJ/kg) [49]. However, this approach is sufficient for an internal comparison within the standard-compliant test fuel series studied. Results are summarized in table 1 and detailed information is given in the supplemental material of this work.

3. Material and methods

This section describes the basic experimental methodology used to determine the emission characteristics of the fuels, i.e., the examined soot indices and a laminar burner to determine the soot threshold, the direct injection engine used to study the particle number emissions, and the flow reactor facility used to measure the soot precursor chemistry. Finally, the correlation analysis applied for comparison and analysis of the different results is presented.

3.1 Soot indices

In this work, we used different soot indices to describe the sooting propensity of the fuels in various combustion environments. On the one hand, sooting tendency indices, like OESI and YSI, are initially measured in diffusion flames. On the other hand, the soot threshold (φ_{ST}) is based on measurements on a premixed laminar flat flame. PMI developed based on engine measurements, including IHD and vapor pressure, completes the set of soot indices. We chose different soot indices to minimize the influence of experimental and simulation variance on subsequent correlations, respectively.

Particulate Matter Index (PMI), for example, could be calculated by the Honda approach [16] according to Eq. (2):

$$\mathrm{PMI} = \sum_i \left(\frac{IHD_i + 1}{VP(443K)_i} \cdot w_i \right) \tag{2}$$

Which includes fuel factors like the IHD and the vapor pressure *VP* at 443 K of each fuel compound *i* weighted by their mass fraction *w*. Oxygen bounded in the fuel molecule and its influence on soot formation is not explicitly considered in the PMI.

For determining the basic sooting tendency of hydrocarbon fuels, smoke point (SP) measurements are a widely used method [17, 50], which is even prescribed as a specification parameter for aviation fuel certification (ASTM D1655). SP represents the flame height of a diffusion-controlled wick flame without a breakthrough of soot. Here, fuel sooting tendency is inversely proportional to SP, i.e., the lower SP is, the more a fuel forms soot. Calcote and Manos [17] derived the apparatus-independent Threshold Soot Index (TSI) for hydrocarbon fuels to minimize the difference between the respective SP measurement sources. The TSI is not adequate for oxygenated fuels because the TSI overestimates their

tendency to soot. Barrientos et al. [18] developed an adaption of the TSI for oxygenated fuels ($C_nH_mO_p$) by dividing the molar stoichiometric oxygen-fuel ratio by SP, namely the Oxygen Extended Sooting Index (OESI):

$$\mathrm{OESI} = a'\left(\frac{n+\frac{m}{4}-\frac{p}{2}}{SP}\right)+b' = a'\frac{MW_{Fuel}}{SP}\left(\frac{w_C}{MW_C}+\frac{w_H}{4\cdot MW_H}-\frac{w_O}{2\cdot MW_O}\right)+b' \quad (3)$$

Where *n, m,* and *p* are the number of carbon, hydrogen, and oxygen atoms per mole of fuel, *MW* is the molar weight, and *w* is the weight proportion of each element in the fuel (C/H/O). Again, the molar weight of the fuel MW_{Fuel} can be calculated by detailed chemical composition data as mentioned before for IHD or can be estimated according to Barrientos et al. [51]. Apparatus-specific constants *a'* and *b'* can be obtained by linear regression analysis of pure compound measurements against TSI literature data [52], assuming that TSI ≈ OESI for oxygen-free hydrocarbons [18].

McEnally and Pfefferle [19] developed the Yield Sooting Index (YSI) experimentally determined by the maximum soot volume fraction $f_{v,max}$ along the centreline of a diffusion flame:

$$\mathrm{YSI} = c\cdot f_{v,max}+d \quad (4)$$

Where *c* and *d* are apparatus-specific constants used to ensure a YSI scale range from 0 to 100. The YSI is a characteristic measure for the tendency of a pure compound or a mixture to produce soot in a combustion environment.

Furthermore, in a consecutive study, McEnally et al. [20] showed that the YSI of a mixture could be calculated following the mixing rule of a linear summary of the individual YSI_i corresponding to each component *i* of the mixture, weighted according to their mole fraction x_i, as given in Eq (5). Therefore, it can be used to predict the sooting propensity of newly developed fuels. Hence, the YSI of a fuel can be simulated when the detailed quantitative composition of a fuel is determined with component accuracy, as is possible, e.g., using comprehensive two-dimensional gas chromatography (GCxGC) [53] following Eq (5).

$$\mathrm{YSI_{Fuel}} = \sum_i (x_i \cdot YSI_i) = \sum_i \left(w_i \cdot \frac{MW_{Fuel}}{MW_i} \cdot YSI_i \right) \quad (5)$$

Here, w_i corresponds to the mass fraction of component i, MW_i to the molecular mass of component i, and MW_{Fuel} to the medium molecular mass of the fuel mixture. Both w_i and MW_{Fuel} can be determined from GCxGC-data.

For the investigated fuel series, PMI was measured by Coryton, England [31] and calculated as described by Aikawa et al. [16] according to Eq. (2). Smoke point (SP) of the test fuels was measured in a standardized wick lamp and published within a previous study [30]. OESI was calculated according to Eq. (3), and the determination of the apparatus-specific constants for OESI (and TSI) calculation is described in the supplemental material. The determination of the YSI as a function of the composition derived from GCxGC is based on the precise identification and quantitation of all individual components present in the fuel blends (for details regarding the GCxGC analysis, see [30]). The YSI was subsequently calculated via Eq. (5), taking the mole fractions and average molecular weights derived from GCxGC-data and the $\mathrm{YSI_i}$ of the individual component from the database created by the Pfefferle research group [54]. Measured YSI is available in the database for about 95 % of the components determined by GCxGC. The remaining 5 % were linearly extrapolated from the nearest available neighbors.

The soot threshold (φ_{ST}) was determined from the measurement of the particle number density in the exhaust gas of a premixed laminar flat flame using a condensation particle counter (CPC 3022A, TSI). In section 5 of the supplemental material and previous publications [55, 56] a detailed description of the measurement, including a scheme of the experimental setup, is given. The measured particle densities were scaled to 10^4 particles/cm^3, and the corresponding value of the fuel-air equivalence ratio (φ) was determined from an exponential function fitted to the data points of each measurement. As a measure of the sooting propensity, the φ value defined as soot threshold (φ_{ST}) is obtained from the gradient at a particle concentration of 10^4 particles/cm^3, by extrapolation to the baseline, as shown in Fig. 4.

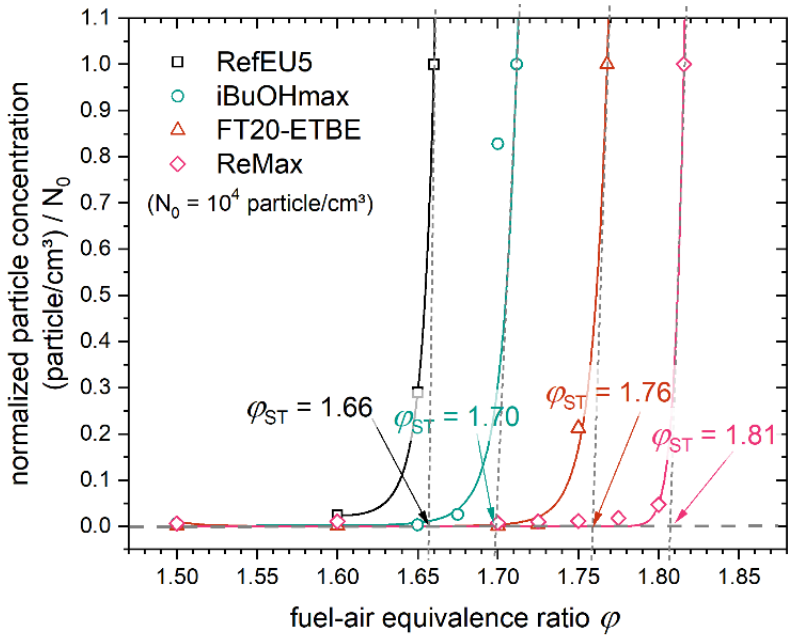

Fig. 4. Normalized particle concentrations for different fuels showing the extrapolation to the soot threshold (φ_{ST}). The grey dashed tangent lines indicate the maximum gradients of the increasing particle concentration and are extrapolated to the baseline where the intersection gives the value for φ_{ST}.

The determination of φ_{ST} is shown as an example for four different fuels. The extrapolation of the tangent line to the baseline (particle concentration below the detection threshold) yields the values of φ_{ST}. The uncertainties are determined from at least three repeated measurements of each fuel and range from ± 0.016 to ± 0.030.

3.2 Test engine

The test engine is a series production turbocharged gasoline direct injection engine with four cylinders (in-line), a displacement of 2 liters, and a centrally mounted Bosch high-pressure injection valve (HDEV6) with fuel pressure up to 350 bar. The engine test bench includes an engine dynamometer with external controllable coolant, fuel, air, and intercooler temperatures. Engine oil temperature is not controlled. This temperature results from constant coolant temperature and a specific load of the operating point. In-cylinder pressures were measured by piezoelectric pressure transducers (Kistler 6041B). Gaseous and particulate engine-out emissions were measured using a Horiba Mexa 7100 and a Horiba SPSC 2100, respectively. PN determination is based on laser scattering condensation particle counting (CPC); the system allows for a counting efficiency of 50 % ±12 % for 23 nm particles, counting efficiency of 41 nm particles is >90 %.

For the PN evaluation of the renewable fuel candidates, three measurement points of the Bosch renewable fuel evaluation program, as published in [7], were chosen. First, PN emissions were evaluated in load sweeps at stationary engine operation in cold and warm conditions. Second, the robustness of the fuel PN emission on Start-of-Injection (SOI) was analyzed by SOI sweeps at low engine speeds and different engine loads. Finally, transient PN emission was analyzed by quasi-digital load steps from idle to wide open throttle load under cold conditions and low engine speed. The operating conditions and parameters of all three program points are listed in Table 2.

Table 2
Engine parameters and conditions of all three tested measurement points.

a) Load sweeps

Parameter	Unit	
Speed	rpm	2000, 4000, 6000
Load (BMEP)	bar	2, 4, 6, 8, 10, 12, 14, 16, 18
Rail pressure	bar	Calibration engine map
Temperature coolant	°C	Cold engine: 25 – 40 Warm engine: 90 – 125
SOI	°CA before TDC	Calibration engine map
Ignition angle	°CA after TDC	Calibration engine map

b) SOI sweeps

Parameter	Unit	
Speed	rpm	1500
Load (BMEP)	bar	2, 10, 18
Rail pressure	MPa	20, 20, 35
Temperature coolant	°C	90
SOI	°CA before TDC	240 – 360, variation in steps 10
Ignition angle	°CA after TDC	Optimized for MFB50 at 8

c) Load steps

Parameter	Unit	
Speed	rpm	1500
Load (BMEP)	bar	Low load: 2.5 High load: 16
Rail pressure	Mpa	35
Temperature coolant	°C	30
SOI	°CA before TDC	290
Ignition angle	°CA after TDC	Optimized for MFB50 at 8
Time at low load	s	135
Time at high load	s	45

Load sweeps were tested at three different engine speeds at warm and cold engine conditions. A load sweep was performed at each engine speed from 2 to 18 bar brake mean-effective pressure (BMEP). Rail pressure, Start-of-Injection (SOI), ignition angle, and other parameters were defined by the calibration data of the engine. It was checked that these parameters were constant for each fuel, meaning that measured PN emission differences can objectively be ascribed to fuel effects. The SOI sweeps were performed at constant engine speed for three different loads. On each load, SOI was varied from 360 °CA to 240 °CA before the top dead center (TDC) in steps of 10 °CA with SOI of 290 °CA as the center.

The ignition angle was optimized for the position where 50 % of the fuel mass fraction is burned (MF B50), and rail pressure was kept constant for each fuel. A quasi-digital step for a continuous time window was performed for the load steps. The engine was run at a low load for 135 s, followed by a high load operation for 45 s. After that, a consecutive new low load and high load cycle followed. The loading pattern was repeated until, in total, six load steps were performed. During each load step, a temporal variation of PN concentration was measured. The first load step was neglected for data evaluation to pre-condition the engine and lose track of measurements conducted before. Hence, five load steps were taken for PN emission evaluation. PN emission signal was averaged, and one load step was chosen closest to the average. This best-fit load step is used for further discussion in this paper.

3.3 Atmospheric laminar flow reactor (ALFR)

The chemistry of the homogeneous gas phase was studied in DLR's atmospheric laminar flow reactor (ALFR) coupled with molecular-beam mass spectrometry (MBMS). The ALFR has been widely used for kinetic studies of combustion chemistry of pure substances [57-59], component mixtures (surrogates and additives) [60], and typical single-molecule alternative fuels, e.g., oxymethylene ethers (OMEs) [61, 62], alcohols [63, 64] and farnesan [44]. In addition, extensive studies have been conducted on the oxidation behavior of real technical fuels, e.g., jet fuels [65, 66] and gasoline [30]. For this work, the speciation data of Zinsmeister et al. [30] are used to analyze the influence of fuel properties on the soot precursor chemistry. A detailed description of the flow reactor facility and the evaluation method is given in [44, 67]. In the following, only selected aspects of the experiment are presented.

In the ALFR experiment, the liquid fuel is pre-vaporized and carried to the flow reactor in high Argon-dilution (Ar > 99 %(v/v)). Control of flow rates is performed by calibrated Coriolis mass flow controllers (Bronkhorst, Mini CORI-FLOW™). In the flow reactor, a well-known temperature profile is imposed on the gas flow running cooling temperature ramps from high to intermediate gas temperatures (1230 – 785 K). A relative accuracy of ±5 K can be assumed. *In-situ* sampling is performed at ambient pressure at the reactor outlet via a quartz nozzle using a differential pump stage (10^{-4} – 10^{-6} mbar). The extracted gas sample is expanded into the high vacuum to suppress further combustion reactions. After applying soft electron ionization (EI; actual energy 11.5 eV), the individual combustion intermediates can be detected based on their mass-to-charge ratio (m/z) in a reflectron time-of-flight mass spectrometer (TOF-MS). Evaluation and quantification of the measured signals were performed according to [67, 68] resulting in uncertainties in mole fractions of 10 – 20 % for species evaluated by direct cold gas calibration and a factor of 2 – 4 for species mole fractions estimated by the relative ionization cross section (RICS) method [69]. From the speciation data set in [30], only the slightly-rich combustion conditions, i.e., the air-fuel ratio of $\lambda = 0.83$, were used in this work. Flowrates of the test fuel series, a schematic of the ALRF facility, and a more detailed description of the used evaluation method are given in the supplement material.

3.4 Correlation matrix of fuel properties

For interpretation of the influence of the various fuel properties as well as the fundamental results from lab experiments, a correlation analysis with the engine PN emissions is performed. For this purpose, the value of a specific fuel property (e.g., evaporated volume fraction at 70 °C, E70) is plotted against the measured PN concentration at a certain engine condition (e.g. at 2 bar BMEP) for all fuels. A least square linear fit is performed and the resulting correlation quality, i.e., the correlation coefficient (R^2) is recorded in a matrix (e.g., 0.2 for E70 vs. 2 bar BMEP). Strong correlations (R^2 close to 1) are color-coded dark while weak correlations (R^2 close to 0) are color-coded white. The respective rounded R^2 is noted in the respective matrix field. The resulting matrix of fuel properties and engine condition then allows for the identification of areas with a strong correlation of a fuel property at a certain engine test condition. This type of analysis is reported for comparing particulate emissions recorded at the load sweep (variation of BMEP, Fig.7), at the SOI sweep (Fig 9), at the load steps (Fig. 11), and for the soot

precursor intermediates (Fig. 12) measured at the atmospheric laminar flow reactor (ALFR). For each analysis, the fuel properties are divided into volatility properties (i.e., relevant values of the distillation data as well as specific and molar ΔH_{vap}) and chemical composition-related properties (i.e., the soot indies and mass fractions of chemical classes abundant in the fuels).

4. Results and discussion

This section examines the fuel effect on the tendency towards soot formation from three sides. In the following, we will look at different fuel parameters of influence. First, the sooting propensity determined from different soot indices is evaluated. Second, engine particulate emissions are assessed. Third, the soot precursor chemistry is investigated in the homogenous gas phase independent of fuel evaporation effects. Finally, those three sets of data and parameter correlations are compared to each other, respectively.

4.1 Soot indices and sooting propensity

Different soot indices described the sooting propensity of the fuels. Fig. 5 shows pair plots of different soot index metrics: PMI, OESI, YSI, soot threshold (φ_{ST}), and IHD. Since a high value of φ_{ST} corresponds to a low propensity to form soot, the reciprocal φ_{ST} value is used. Linear least square fits (dashed lines) are applied, and the corresponding correlation coefficients of determination (R^2) are also given. Note that φ_{ST} was not measured for the complete fuel set.

As shown in Fig. 5, linear least square regression between each pair of the soot indices OESI, YSI, and PMI, prove a linear correlation of these indices, with a coefficient ranging from $R^2 = 0{,}92$ up to $R^2 = 0.99$. The correlation of the three indices with IHD is less strong (R^2 from 0.75 to 0.98). The correlation of all indices with laminar flat flame-based soot threshold (φ_{ST}) ($R^2 = 0.66 – 0.81$) is the weakest but still clearly visible. The linear correlations of each pair of PMI, OESI, and YSI for the entire series of fuels give the best results. This is of particular interest since the three indices use independent properties as divisors, i.e., the PMI is the quotient from the division of the IHD and the vapor pressure of individual compounds. In contrast, the OESI divides the smoke point by the stochiometric oxygen demand. Finally, the YSI reflects the respective fuel compounds' mole fraction weighted sooting

propensity. All three indices are designed to reflect the sooting behavior of diffusion flames. Less stringent correlations exist for the IHD and φ_{ST}, neither associated with diffusion flames.

The group of fuels with approximately the same high amount of aromatics ($w_{Aromatics}$ = 35 – 41 %(m/m)), namely RefEU5Cert, MTBEmax, ETBEmax, iBuOHmax, FT(18)MTBE, and FT(20)ETBE, form a cloud of measuring points for most of the soot indices. The reference fuel has one of the highest sooting propensities for almost every index. This is not unexpected since it has the lowest oxygen content of 1.76 %(m/m) alongside the highest aromatics content of 40.8 %(m/m). It is noteworthy that the PMI lists the MTBEmax as the most sooting fuel.

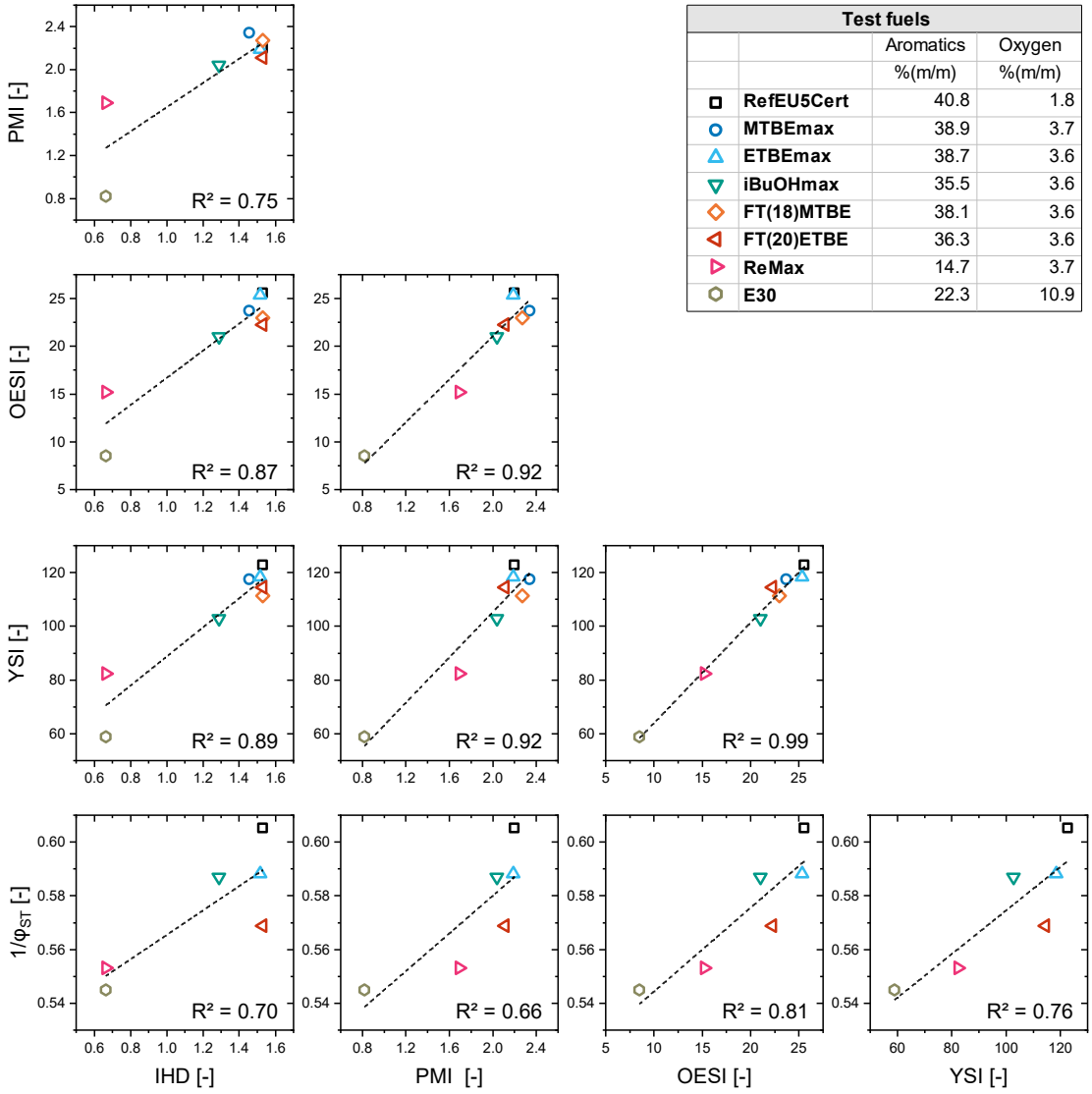

Test fuels			
		Aromatics	Oxygen
		%(m/m)	%(m/m)
☐	RefEU5Cert	40.8	1.8
○	MTBEmax	38.9	3.7
△	ETBEmax	38.7	3.6
▽	iBuOHmax	35.5	3.6
◇	FT(18)MTBE	38.1	3.6
◁	FT(20)ETBE	36.3	3.6
▷	ReMax	14.7	3.7
⬡	E30	22.3	10.9

Fig. 5 Pair plot of different soot index metrics: Particulate Matter Index (PMI), Oxygen Extended Sooting Index (OESI), Yield Sooting Index (YSI), reciprocal value of soot threshold (φ_{ST}), and Hydrogen Deficiency Index (IHD). Linear least square fits are given as dashed lines. (R^2 = coefficient of determination).

The oxygen amount of the other standard-compliant fuels is about ~ 3.6 %(m/m), very similar and close to the upper limit of the DIN EN 228 specification. The lower sooting propensity of this bulk of fuels is represented by iBuOHmax, for almost all indices, i.e., PMI, OESI, YSI, and IHD. In contrast, φ_{ST} shows a lower soot propensity for the FT(20)ETBE.

ReMax and E30 are the fuels with the lowest sooting propensities, while the sooting propensity of ReMax is determined to be higher than E30 for all soot indices. The oxygen content of the ReMax fuel is similar to the fuel mixtures considered before. Still, it has a lower total aromatics concentration ($w_{Aromatics}$ = 15 %(m/m)), leading to a lower sooting propensity. Although the E30 fuel has a higher amount of aromatics ($w_{Aromatics}$ = 22 %(m/m)) than the ReMax fuel, it exhibits the lowest sooting propensity. It seems evident that the higher aromatics concentration is compensated by, the higher oxygen content of about 11 %(m/m). The effect of oxygen content on soot oxidation has already been reported, e.g., [70, 71]. A closer look at the fuel composition reveals that the type of aromatics may also affect the results. Most of the aromatics in E30 are composed of 8 C-atoms, while in ReMax, most aromatics are higher than C9.

Even though all soot indices considered to capture the sooting propensity for this fuel pair (ReMax and E30), notable differences can be observed: IHD and φ_{ST} indicate a sooting propensity very close to each other, while the other indices differ significantly for these fuels. For IHD, the insensitivity to the oxygen content is not surprising since no double bound is formed and counted by OH groups of alcohol. In principle, the soot threshold φ_{ST} as a measured value considers all fuel characteristics. It should be noted that the respective flames are designed for a constant gas velocity leading to a lower fuel flow rate for ReMax since a lower amount of substance is required for a gas volume, being comparable to the other fuels. For the same reason, different flame temperatures can be expected for the various fuels that are not compensated when determining the φ_{ST}.

4.2 Particle number (PN) engine emissions

This chapter discusses the results of the three sets of tests: Load sweep, SOI sweep, and load steps.

Load sweep. Six sets of stationary load sweeps at different engine speeds (2000/4000/6000 rpm) with the cold and warm engine were conducted to assess a general dependency of PN emissions on the engine

load and engine temperature in the calibrated engine map. In Fig. 6, the engine out PN concentration for engine load in a range of 2 – 18 bar BMEP is shown for a cold and warm engine, comparing the fuel candidates. Due to experimental issues, E30 measurement is not available for 2000 rpm, warm engine.

At a warm engine and 2000 rpm (a), the lowest PN emissions (< one order of magnitude) can be seen for ReMax in the tested load range in comparison to the other fuel candidates. Whereas, at 4000 rpm (b), all the fuels behave more similarly, with ReMax at the lower end of the data set. Similar behavior can be found at 6000 rpm for ReMax fuel (c). At these two engine speeds, the fuel properties may play a subordinate role in PN emissions, which will be discussed later. For 4000 rpm (e) and 6000 rpm (f) and cold engine, the PN emission behavior for the different fuels is similar to the warm engine. No significant differences between the fuel candidates can be measured. For 2000 rpm and cold engine (d), fuel differences in PN emissions become more apparent, with ReMax and E30 showing the lowest PN concentration.

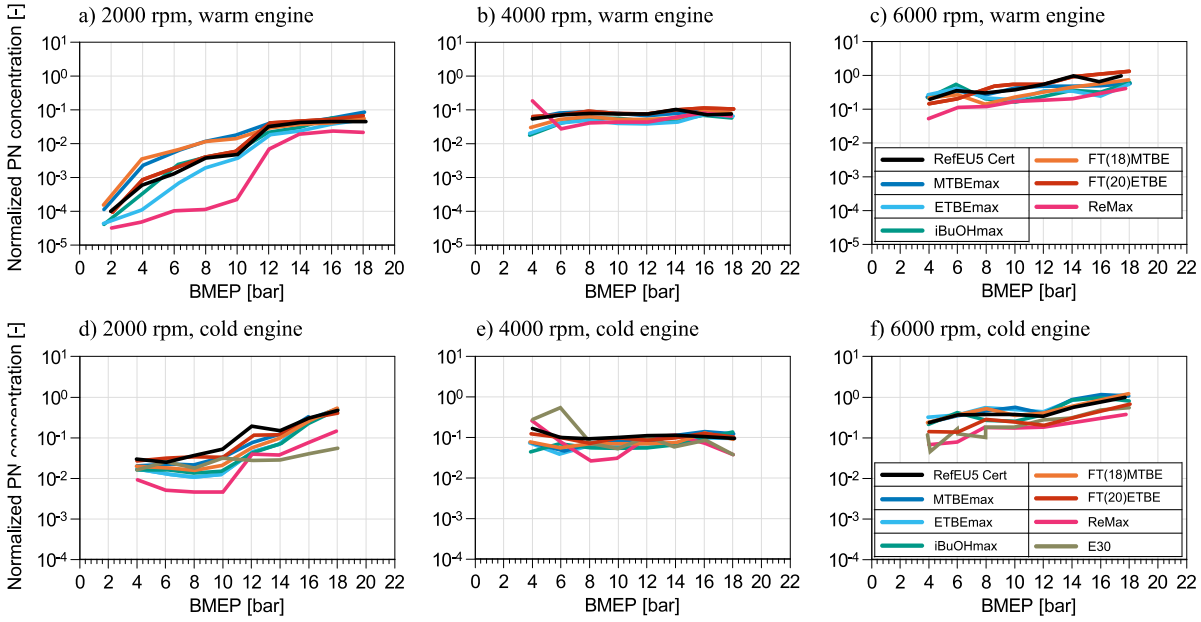

Fig. 6. Normalized engine out particulate number (PN) concentration for load sweeps at 2000/4000/6000 rpm. Absolute PN concentration is normalized on the maximum value of RefEU5Cert fuel at 6000rpm and each temperature set. Top: Warm engine operation, coolant temperature: 90 °C. Bottom: Cold engine operation, coolant temperature: 25 – 40 °C.

It is known that PN engine emissions can be influenced by fuel properties, especially during cold start [41]. Therefore, in more detail, we examined the cold engine load sweeps at 2000 rpm. Measured data are correlated with fuels' properties, and the coefficient of determination R^2 assesses the goodness of the least square linear fit. Fig. 7 pictures the correlation matrix between PN (2000 rpm, cold engine) and

fuels' volatility and chemical composition properties, respectively. Dark-colored areas indicate a strong correlation, while the actual coefficients of determinations (R^2) are given in the colored rectangles. The data shows the best correlation between PN emission and fuel properties for engine loads greater than 12 bar BMEP. At the same time, the highest correlation can be found for chemical fuel composition, such as soot indices and aromatics content. Remarkably, E30 fuel exhibits higher PN emissions at loads < 12 bar BMEP than ReMax. Other effects may dominate the particle formation here, which are not described by the analyzed fuel parameters. Although mostly enthalpy of evaporation (ΔH_{vap}) is named as the root cause for higher soot emissions of ethanol-containing fuels [72, 73], this study cannot confirm this. The ΔH_{vap} correlation coefficient is relatively low for all engine loads tested.

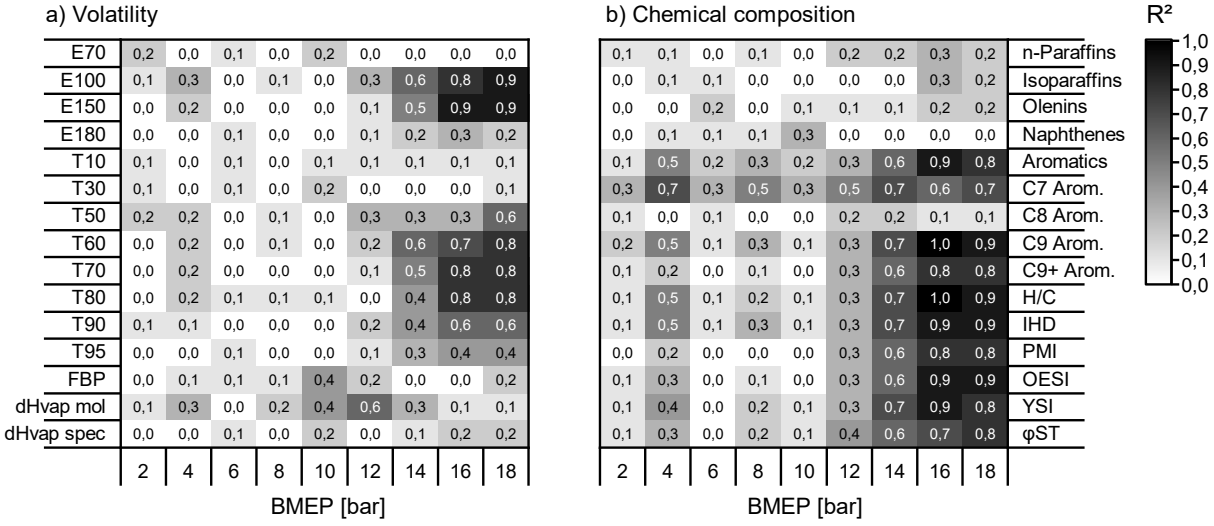

Fig. 7. Load sweeps correlation matrices between PN (2000 rpm, cold engine) and fuels' (a) volatility and (b) chemical composition, respectively. (R^2 = coefficient of determination).

Start of injection (SOI) sweep. SOI sweeps are performed to challenge the effect of engine injection timing on PN emissions. Especially early or late injection timing could lead to liquid fuel wall films, where specific fuels could react with increasing PN emissions depending on their fuel properties. The results for different SOI on PN emission concentration are presented in Fig. 8. Three engine loads at a speed of 1500 rpm and a warm engine (T-coolant: 90 °C) were compared. At each load, the SOI was swept between 240 °CA and 340 °CA before the top dead center, with calibrated SOI at 290 °CA. Note that running smoothness is reduced (COV was measured between 3 – 5 % independent of the tested fuel candidate) at 2 bar BMEP, which results in higher PN fluctuation. Therefore, differences in PN emission should not be interpreted and correlated with fuel properties.

At 10 bar BMEP, the PN concentration shows a similar picture as in the load sweep measurement (c.f. Fig. 6 a). Most tested fuels behave similarly and are grouped at higher PN levels except ReMax. At this load, E30 is also located in the group of fuels showing higher PN concertation. Whereas most fuels show increased PN emissions at early SOI (e.g., 340 °CA), ReMax and E30 do not show this behavior. PN emission seems less sensitive on SOI for those two fuel candidates. This insensitivity can be seen especially at high engine load (c.f. Fig. 8 c). At 18 bar BMEP, ReMax and E30 also exhibit the highest PN emission reduction.

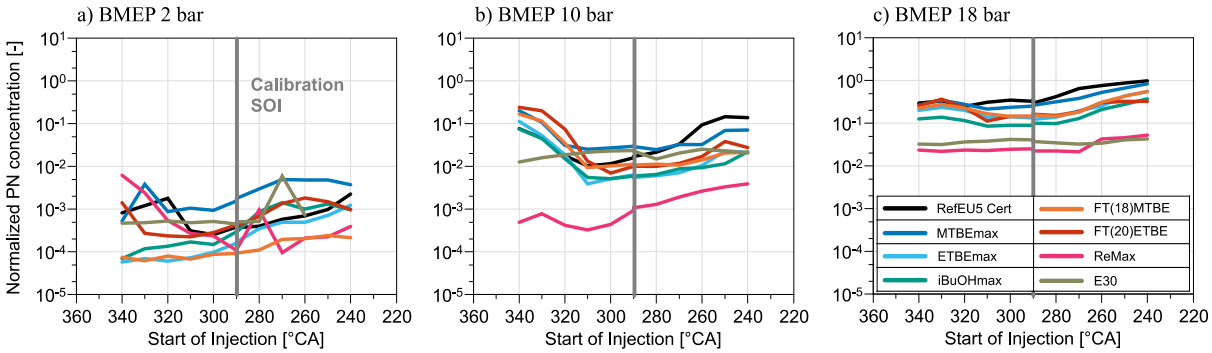

Fig. 8. Normalized engine out PN concentration for SOI sweeps at 1500 rpm and different engine loads. Absolute PN concentration is normalized on the maximum value of RefEU5Cert fuel at 18 bar BMEP. a) Low engine load 2 bar BMEP. b) Moderate engine load 10 bar BMEP. c) High engine load 18 bar BMEP.

In Fig. 9, the corresponding correlation matrices between PN and fuels' volatility and chemical composition are shown for the SOI sweep. Note that the correlation matrix for 2 bar BMEP is not shown due to low combustion smoothness as described above. At medium load (10 bar BMEP), no clear correlation between engine out PN emission and the fuel parameters can be seen. The highest coefficients of determination ($R^2 \sim 0.7$) can be found for volatility parameters such as ΔH_{vap} mol, T30, and E70. However, at high engine load, the chemical composition seems to have a greater impact on engine out PN emissions, as total aromatics, heavy aromatics, and soot indices correlate best with coefficients of determination ($R^2 > 0.7$). It can be noted that the highest coefficients of determination can be found at early SOIs (340 °CA) and late SOIs (240 °CA). It seems that especially the chemical composition shows a higher impact on PN emission at injection timings, where homogenization time is reduced (e.g., 240 – 250 °CA) or components are exposed to liquid fuel as the injection takes place when the piston is near the top dead position (e.g., 320 – 340 °CA). At injection timings near the calibration value (290 °CA), the fuel property effect on PN emission may be subordinated at high engine load.

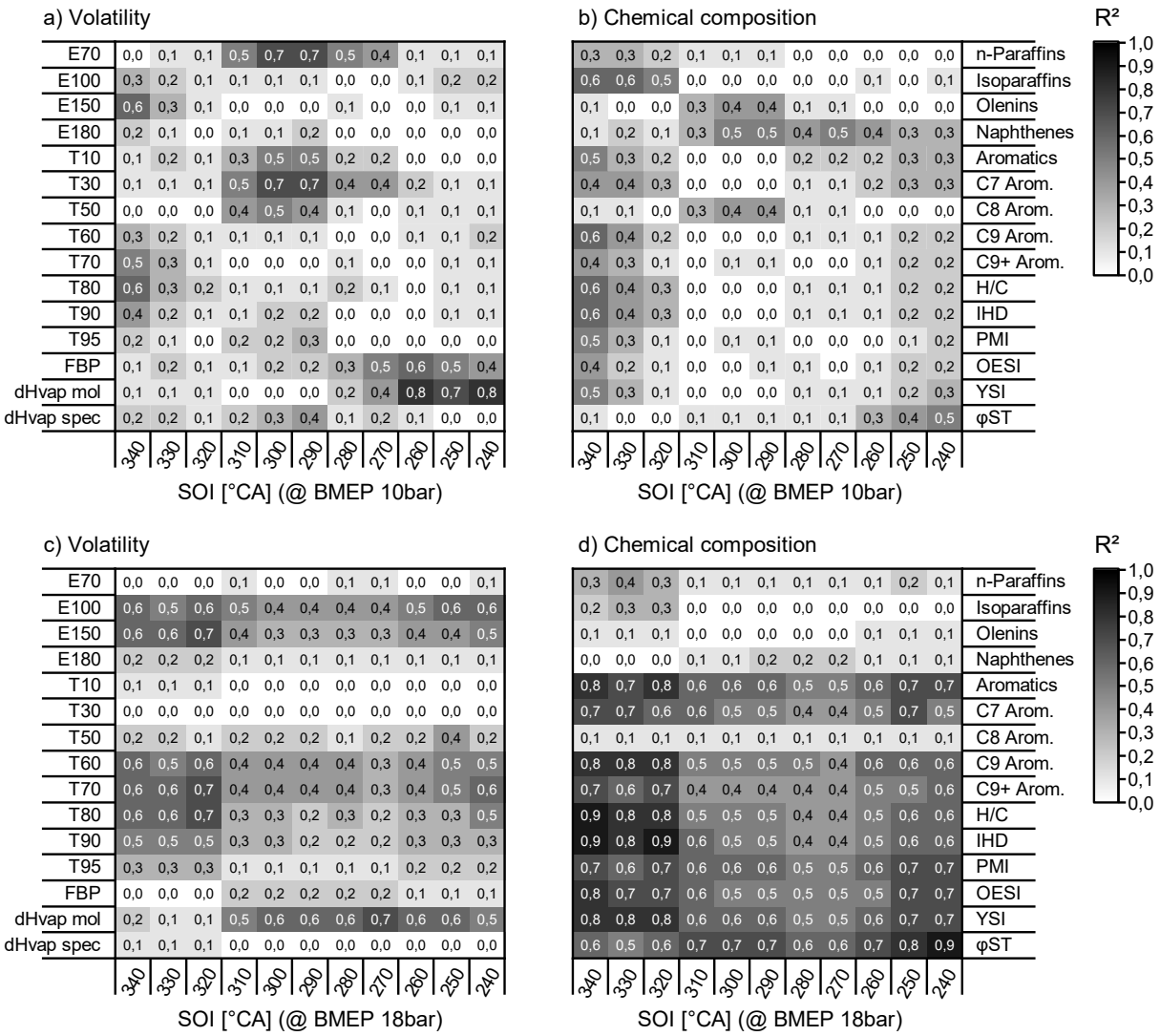

Fig. 9. SOI sweeps correlation matrices between PN (1500 rpm, cold engine) and fuels' (a/c) volatility and (b/d) chemical composition, respectively. Top: SOI @ 10 bar BMEP, Bottom: SOI @ 18 bar BMEP. (R^2 = coefficient of determination).

Load steps. Besides stationary operation, the load step measurement represents the dynamic reaction of engine out PN emissions on a rapid increase in engine load. These measurements extend the evaluation of the fuel candidates on PN emission under transient engine operation. In Fig. 10, left the PN emission reaction of the engine is shown. At 20 s, PN concentration increases due to high load demand. After that, the steady high load phase follows, where the PN signal remains at higher concentration values. However, the peak when reaching high load condition can be found at each fuel's beginning of the load step (between 20 – 30 s). Peak and average values (between 20 – 40 s) for each fuel are drawn in a separate diagram in Fig. 10, right.

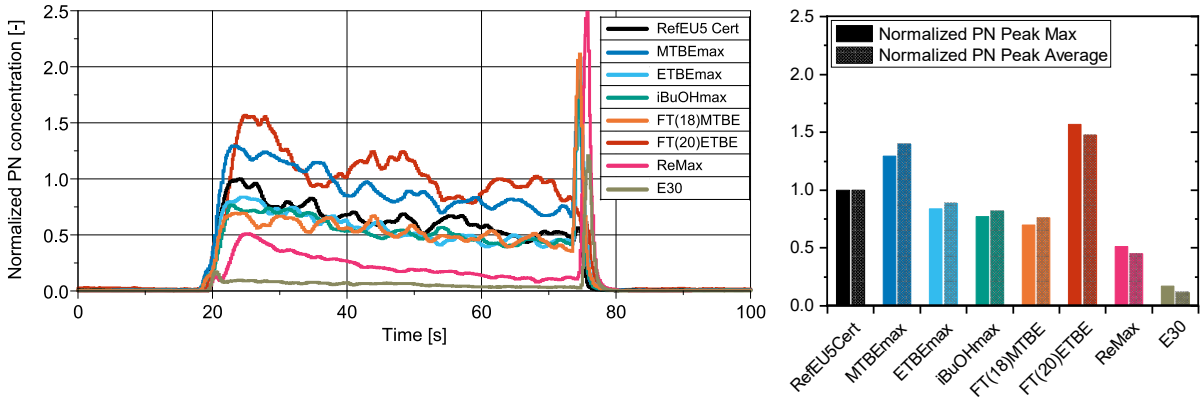

Fig. 10. Left: Normalized engine out PN concentration for load steps at 1500 rpm (cold engine, coolant temperature 30°C). Right: Normalized PN peak maximum and PN average (window: 20 – 40 s). Absolute PN concentration is normalized on the peak value of RefEU5Cert fuel between 20 and 40 s for both graphs.

517 In both temporal PN concentration and peak/average concentration, MTBEmax and FT(20)ETBE
518 exhibit the highest PN emissions of the fuel set. At the same time, ReMax and E30 show the lowest PN
519 emission in the dynamic load step. The correlation map (Fig. 11) indicates the chemical composition
520 (e.g., heavy aromatics, soot indices), as well as the boiling curve between the mid and high boiling range
521 (e.g., E150, T70), governing the PN emission behavior of the fuels. For example, ReMax exhibits the
522 lowest boiling curve between 100 – 150 °C and the lowest aromatics content.

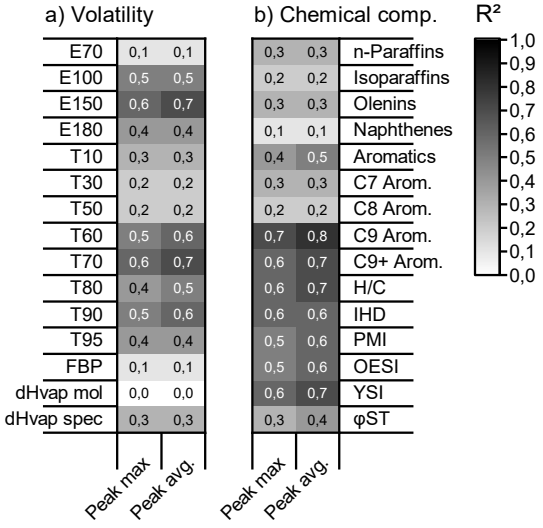

Fig. 11. Load steps correlation matrices between PN (peak maximum and peak average) and fuels' a) volatility and b) chemical composition, respectively. (R^2 = coefficient of determination).

523 In summary, two main fuel groups were identified in the engine experiments. The first group exhibits
524 high PN emissions, including RefEU5Cert, MTBEmax, ETBEmax, iBuOHmax, FT(18)MTBE, and

525 FT(20)ETBE. Since the renewable fuel candidates were designed with similar boiling behavior and
526 heavy aromatic target as RefEU5Cert, this clearly shows that the fossil base fuel content is determining
527 the sooting behavior (mainly aromatics content) of the fuel instead of the amount and type of renewable
528 component. This is in line with the expectations drawn from all discussed soot indices. Even though the
529 order of fuels varies slightly for the different indices, i.e., PMI, OESI, YSI, φ_{ST}, and IHD, the similarity
530 of PN emission for different engine operating conditions is confirmed for this set of fuels. The second
531 group includes ReMax and E30, which have shown significantly lower PN emissions. Again, this
532 finding aligns with expectations based on the soot indices. The fuel sooting behavior can be attributed
533 primarily to the chemical fuel composition with a low aromatics content and significantly fewer heavy
534 aromatics (C9+ aromatics). In transient engine operating points and under conditions with a high
535 probability of mixture inhomogeneities or piston/liner wetting, volatility properties from the mid to end
536 boiling range (e.g., E150) become apparent as a reason for PN emission behavior. Contrary to the
537 expectation, enthalpy of evaporation did not show a high correlation with PN engine out for ethanol
538 containing fuel E30. Further insight into the composition effects of the tested fuels on soot formation
539 will be given in the following chapter.

540 *4.3 Soot precursor chemistry*

541 To assess the fuel composition effects on the soot precursor chemistry, we correlated fuel properties to
542 the maximum mole fraction of selected benzene and soot precursors already published in [30]. The
543 maximum mole fractions were measured at slightly-rich combustion conditions in DLR's atmospheric
544 laminar flow reactor coupled with MBMS spectrometry. The formation of the first aromatic ring
545 structure is often cited as crucial in the soot precursor chemistry, e.g., [9-13]. Typical benzene build-up
546 species from the degradation of hydrocarbon fuels are small intermediates like acetylene (C_2H_2),
547 allene/propyne (C_3H_4), vinyl acetylene (C_4H_4), butadiene (C_4H_6), and cyclopentadiene (C_5H_6). Further
548 reaction of benzene with these small build-up species, among others, can lead to the formation of
549 polycyclic aromatic hydrocarbons (PAHs), which also play an essential role in soot precursor chemistry.

550 Linear least square correlation matrices between maximum mole fractions ($x_{i,max}$) of previously named
551 small benzene build-up species, as well as selected aromatic soot precursor species and
552 volatility/chemical composition characteristics of the gasoline blends, are shown in Fig. 12. Mono-

aromatics such as benzene (C_6H_6) and indene (C_9H_8), as well as PAHs like acenaphthylene ($C_{12}H_8$), fluorene ($C_{13}H_{10}$) and phenanthrene ($C_{14}H_{10}$), were chosen as aromatic soot precursors as examples. Again, dark-colored areas indicate a strong correlation, while the actual coefficients of determinations (R^2) are given in the colored rectangles. As for the engine correlation matrices, the left plot images the soot precursors' correlation to fuels' volatility, while the right plot allows interpretation of the correlation to fuels' chemical composition.

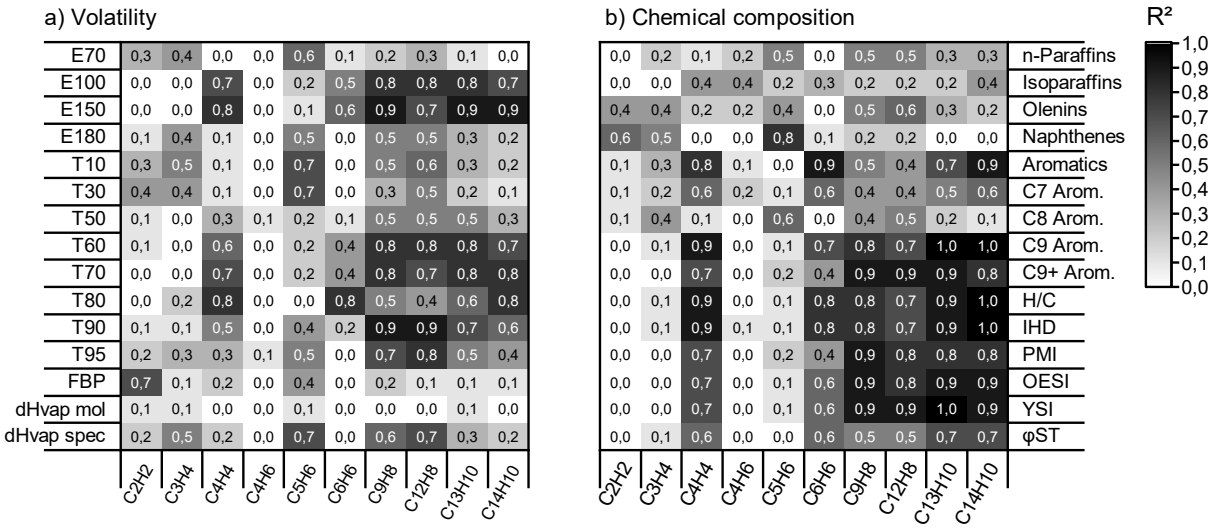

Fig. 12. Soot precursors correlation matrices between maximum mole fraction and fuels' a) volatility and b) chemical composition, respectively. (R^2 = coefficient of determination).

In Fig. 12 b), high correlation coefficients of determination ($R^2 = 0.78 – 0.96$) between aromatic species larger than benzene (C_9H_8, $C_{12}H_8$, $C_{13}H_{10}$, and $C_{14}H_{10}$) and soot indices (PMI, OESI, YSI, and φ_{ST}) indicate that soot formation is already caused in the gas phase by higher condensed aromatic species. As in a previous comprehensive study of jet fuel combustion kinetics [65], benzene (C_6H_6) does not appear to be the best indicator of soot formation within the species pool of soot precursors for oxygenated types of gasoline as well. Among the smaller build-up species, only vinyl acetylene (C_4H_4) shows a clear correlation to the soot indices ($R^2 \approx 0.7$), whereby correlation to H/C and IHD is even more pronounced ($R^2 \approx 0.9$). As a measure of the lack of hydrogen, the IHD (or H/C) indicates the unsaturation of a fuel. In principle, like aromatics, polyunsaturated hydrocarbons form more soot than saturated hydrocarbons such as paraffins [17]. It is, therefore, not surprising that there is a strong correlation between the aromatic composition of the fuels and the soot precursor species formed.

570 As for engine PN emissions, correlations with fuel volatility (Fig. 12 a)) also occur for the investigated
571 soot precursors. The correlation between aromatic soot precursor species and distillation data
572 E100/E150 and T70/T80/T90 appears relatively strong ($R^2 = 0.7 – 0.9$). However, since the
573 measurements of soot precursor chemistry take place with pre-evaporated fuel in the homogenous gas
574 phase, the influence of the fuels' volatility behavior is excluded. Therefore, this can only be a matter of
575 correlations whose causality is influenced by fuel chemistry.

576 Distillation data such as T80/T90 and E150 mentioned fuel properties that affect PN engine emissions
577 (e.g., [42]). They represent the upper boiling end of a substance and are significantly influenced by fuel
578 composition. We have taken a closer look at the composition of the upper boiling end, more precisely
579 at the theoretical residual volume fraction of 20 %, which corresponds to the T80 point. Note that the
580 T80 volume fraction was taken from the two-dimensional gas chromatography data, not from a real
581 distillation process. Thus, effects such as under and over-attraction are not considered. For example, the
582 chemical composition of the T80 volume fraction of the reference fuel RefEU5Cert as well of the fuel
583 candidates ReMax and E30 is shown as weighted bar charts divided into the hydrocarbon groups: *n*-
584 paraffins, isoparaffins, olefins, cycloparaffins and aromatics in Fig. 13. Moreover, the mono-aromatics
585 group is broken down to the number of C-atoms. For the investigated test fuels, T80 points lie in a
586 temperature range of 110 – 160 °C, which is why species smaller than C8 are almost absent from the
587 T80 volume fraction, and mono-aromatics with C8 to C11 atoms dominate the T80 composition overall.

588 As we have already pointed out in our previous publication [30], soot precursor chemistry is a highly
589 complex process. Simple correlations such as more aromatics in a fuel cause higher soot precursor
590 concentration are only sometimes valid for highly complex fuel mixtures. Predominant PAH formation
591 pathways of different aromatic fuel components are discussed below, each based on a representative
592 species of C7, C8, C9, and C10 aromatics. Starting with toluene (C_7H_8), *p*-xylene (C_8H_{10}),
593 1,2,4-trimethylbenzene (C_9H_{12}), and ending with polymethylated 1,2,4,5-tetramethylbenzene ($C_{10}H_{14}$).

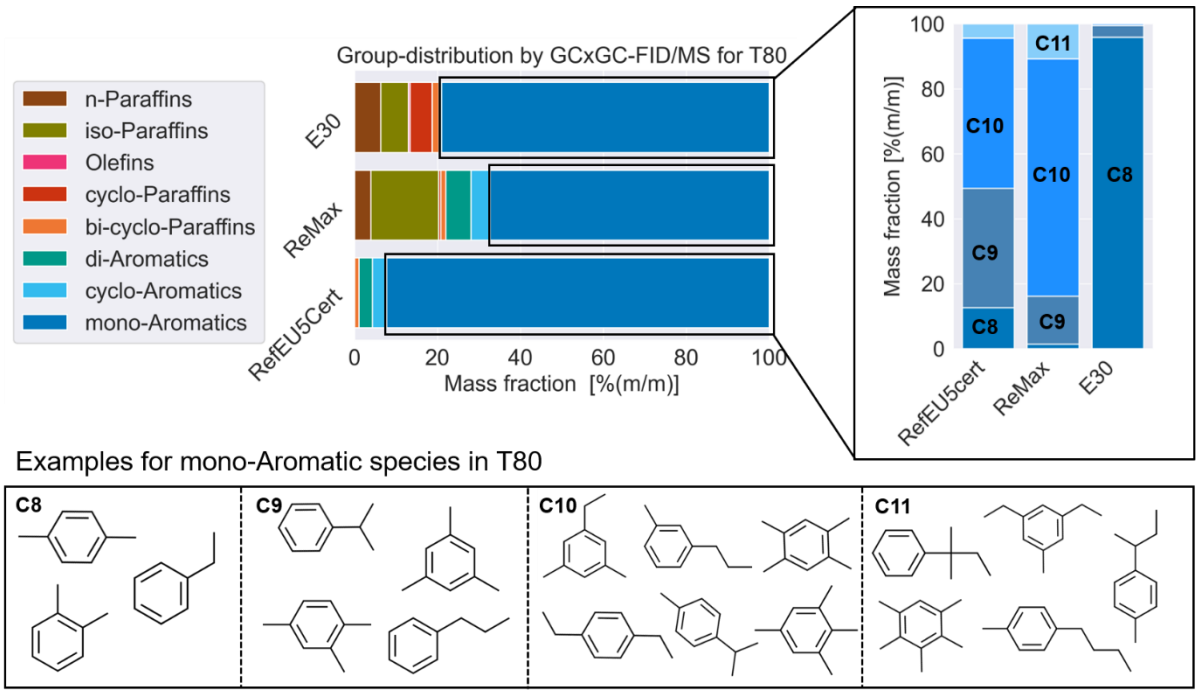

Fig. 13. Chemical composition of remaining not evaporated fuel volume fraction at T80 of the reference gasoline RefEU5Cert, and the test fuels ReMax and E30.

Yuan et al. [74, 75] stated that PAH formation during toluene pyrolysis occurs via fuel consumption products such as $C_6H_6CH_2$, C_7H_6, C_6H_6, and C_5H_6, among others. Investigation of benzene-propyne and toluene-propyne flames of Hansen et al. [76, 77] show that molecular growth is mainly driven by recombination reactions of radicals, ring closure, and ring enlargement reactions, while fuel-structure has only minor influence. For *p*-xylene, C8-chemistry involving species like styrene, styryl, and phenylacetylene plays an important role. However, PAH formation pathways related to benzene/toluene can be considered for C_8H_{10} as well since toluene is one of the main decomposition products of xylene isomers [78, 79]. In studies of alkylbenzene isomers, it was shown that the tendency to soot depends on the number of substituents; e.g., trimethylbenzene tended to form more soot than ethyl toluene [80]. Metathesis of 1,2,4-trimethylbenzene gives dimethyl benzyl radicals, which react further but are not entirely degraded to benzene [81]. Similar assumptions can be adapted to the C10 mono-aromatics, e.g., for $C_{10}H_{14}$ isomers. It can be expected that polymethylated 1,2,4,5-tetramethylbenzene will promote soot formation more than *n*-butylbenzene. Overall, for higher-substituted aromatics, in our case, C9/C10 mono-aromatics, degradation down to benzene will play only a minor role in PAH formation.

This explains why E30 has a lower concentration of high molecular weight soot precursors than the ReMax, despite a higher total aromatics content. This difference is also well reflected by the majority

of soot indices and the PN emissions at fuel-sensitive engine conditions. For E30, the most significant aromatic fractions are C8 aromatics. In contrast, for ReMax and the other test fuels, the C9 aromatics make up the majority of the total aromatics content, which is also reflected in the composition of the T80 volume fraction in Fig. 13. It can thus be shown that the correlation to distillation parameters (especially to the upper boiling end values E150 and T80/T90) is an effect of the chemical composition rather than an evaporation effect. However, they are considered volatility characteristics. On this basis, the correlation between PN emissions and fuels' volatility, shown in Fig. 7 for load sweeps, Fig. 9 for SOI sweeps, and Fig. 11 for load steps, could also be attributed to the chemical composition of the fuels, especially of the upper boiling end of the fuels.

5. Conclusion

This study investigated fuel effects on emission characteristics of six real technical drop-in renewable gasoline fuel candidates compliant with DIN EN 228 and one ethanol/gasoline blend focused on soot formation. First, the sooting propensity of the fuels was assessed using different soot indices. Second, particle number (PN) emissions were measured on a series production turbocharged gasoline direct injection engine with four cylinders. Third, soot precursor chemistry was investigated using a laminar flow reactor at atmospheric pressure and a slightly-rich air-fuel ratio of $\lambda = 0.83$. Finally, correlations to fuel volatility and chemical characteristics were made for the complete data set.

Good correlations between the soot indices were found for the Particulate Matter Index (PMI), the Oxygen Extended Sooting Index (OESI), and the Yield Sooting Index (YSI) for all fuels. This is of particular interest since the related division of these indices differs significantly. However, within the narrow band of the DIN EN 228, all indices provide useful predictions of the fuels' sooting propensity. Engine exhaust measurements are in line with expectations resulting from the soot indices: Fuels with a similar composition of heavy aromatics (C9/C9+ aromatics) and soot indices (PMI, OESI, and YSI) have an equivalent level of engine out PN emission in stationary engine operation, in engine maps at different loads, and engine speeds. However, for most investigated engine conditions, slight differences in fuel properties cannot be distinguished in engine PN concentration measurements.

The picture drawn by soot indices and PN engine exhaust measurements is completed by examination of the soot precursor chemistry in the homogeneous gas phase. It can be concluded that engine PN emissions for the test conditions (e.g., limited evaluation under transient conditions) and the tested fuel candidates are primarily influenced by fuel chemistry. In particular, the composition of the hydrocarbon fraction is decisive, with the heavy C9/C9+ aromatics and the upper distillate significantly impacting soot formation. The apparent PN dependence on evaporation parameters such as E100 and E150 thus represents a correlation rather than causality since the evaporation properties of a fuel blend are significantly influenced by its composition and the contribution of the individual components. For the unique fuels investigated herein, the following summary can be drawn in compliance with all examined fuel properties, from fuel chemistry to engine-out PN emissions:

- ReMax and E30 allow significantly reduced engine-out PN emissions due to their composition.
- Among the DIN EN 228 compliant fuels, ReMax, with the highest renewable content, enables significant PN reduction. The base fuel composition and not the renewable content gain primary influence on PN emissions.
- Enthalpy of vaporization (ΔH_{vap}) does not significantly correlate with the engine-out PN concentration under the tested operating points and conditions.
- Higher boiling end parameters are not directly responsible for increased sooting propensity but are a measure for large aromatics. C9/C9+ aromatics indeed increase soot formation independent from boiling behavior.
- No apparent influence of the structure of the renewable oxygenated component, i.e., alcohol or ether, on soot formation.

In summary, this work highlights the impact of chemical fuel composition, especially the late middle distillate, i.e., primarily heavy C9/C9+ aromatics, as the decisive influence of the tendency to form soot of a molecular complex fuel. Contrarily, it was found that the vaporization behavior of the fuel only plays a subordinate role inside the limitations mentioned above.

6. Acknowledgement

Funding: This work was supported by the German Federal Ministry for Economic Affairs and Climate Action (BMWK) [03EIV221]. The authors thank Romain Palka for supporting the sooting threshold measurements (φ_{ST}) during his internship. The authors thank Thomas Bierkandt most sincerely for his excellent professional support and Stefanie Werner for her experimental contribution.

References

[1] (IEA) IEA. European Union 2020 energy policy review. *IEA Energy Policy Reviews.* Paris: OECD Publishing; 2020:310.

[2] (OPEC) OotPEC. World oil outlook 2045. Vienna: Organization of the Petroleum Exporting Countries (OPEC); 2021.

[3] Hartung S. Antriebsstränge der Zukunft: Wie wir unsere Klimaziele durch Technologieoffenheit erreichen. *42. Internationales Wiener Motorensymposium.* 2021.

[4] Krämer H, Borovsky J, Bulc A. Hochoktaniger paraffinischer Ottokraftstoff innerhalb EN228 E5. In: Krahl J, Munack A, Eilts P, Bünger J, editors. Fuels Joint Research Group, Kraftstoffe für die Mobilität von Morgen. Cuvillier Verlag; 2021, p. 63-70.

[5] Garbe T, Noack B. Measures to increase the CO2 reduction potential of renewable fuels in the period up to 2030. *9th International engine congress.* Baden-Baden; 2022.

[6] Wouters C, Lehrheuer B, Pischinger S, Seifert P, Raabe T, Kolbeck M, et al. Evaluation of synthetic gasoline fuels and alcohol blends in a spark-ignition engine. SAE International Journal of Fuels and Lubricants 2022;15(3).

[7] Krämer H, Send M, Gessner M, Storch M, Kunz T, Geiler JN. Drop-in renewable gasoline fuels for CO2 reduction: Evaluation and demonstration of functional potentials. *9th International engine congress.* Baden-Baden; 2022.

[8] Kulzer AC, Deeg HP, Villforth J, Schwarzenthal D, Schilling M, Barrientos E, et al. Sustainable mobility using fuels with pathways to low emissions. SAE International Journal of Advances and Current Practices in Mobility 2020;2(2020-01-0345):1870-92.

[9] Frenklach M. Reaction mechanism of soot formation in flames. Physical Chemistry Chemical Physics 2002;4(11):2028-37.

[10] McEnally CS, Pfefferle LD, Atakan B, Kohse-Höinghaus K. Studies of aromatic hydrocarbon formation mechanisms in flames: Progress towards closing the fuel gap. Progress in Energy and Combustion Science 2006;32(3):247-94.

[11] Hansen N, Cool TA, Westmoreland PR, Kohse-Höinghaus K. Recent contributions of flame-sampling molecular-beam mass spectrometry to a fundamental understanding of combustion chemistry. Progress in Energy and Combustion Science 2009;35(2):168-91.

[12] Hansen N, Schenk M, Moshammer K, Kohse-Höinghaus K. Investigating repetitive reaction pathways for the formation of polycyclic aromatic hydrocarbons in combustion processes. Combustion and Flame 2017;180:250-61.

[13] Baroncelli M, Mao Q, Galle S, Hansen N, Pitsch H. Role of ring-enlargement reactions in the formation of aromatic hydrocarbons. Physical Chemistry Chemical Physics 2020;22(8):4699-714.

[14] Martin JW, Salamanca M, Kraft M. Soot inception: Carbonaceous nanoparticle formation in flames. Progress in Energy and Combustion Science 2022;88.

[15] Bockhorn H. Soot formation in combustion: Mechanisms and models. *Springer Series in Chemical Physics.* Berlin, Heidelberg: Springer; 1994.

[16] Aikawa K, Sakurai T, Jetter JJ. Development of a predictive model for gasoline vehicle particulate matter emissions. SAE International Journal of Fuels and Lubricants 2010;3(2):610-22.
[17] Calcote HF, Manos DM. Effect of molecular-structure on incipient soot formation. Combustion and Flame 1983;49(1-3):289-304.
[18] Barrientos EJ, Lapuerta M, Boehman AL. Group additivity in soot formation for the example of C-5 oxygenated hydrocarbon fuels. Combustion and Flame 2013;160(8):1484-98.
[19] McEnally CS, Pfefferle LD. Improved sooting tendency measurements for aromatic hydrocarbons and their implications for naphthalene formation pathways. Combustion and Flame 2007;148(4):210-22.
[20] McEnally CS, Xuan Y, St John PC, Das DD, Jain A, Kim S, et al. Sooting tendencies of co-optima test gasolines and their surrogates. Proceedings of the Combustion Institute 2019;37(1):961-8.
[21] Chaos M, Zhao Z, Kazakov A, Gokulakrishnan P, Angioletti M, Dryer FL. A PRF+Toluene Surrogate Fuel Model for Simulating Gasoline Kinetics. 2007.
[22] Chen B, Wang Z, Wang J-Y, Wang H, Togbé C, Alonso PEÁ, et al. Exploring gasoline oxidation chemistry in jet stirred reactors. Fuel 2019;236:1282-92.
[23] Shao C, Kukkadapu G, Wagnon SW, Pitz WJ, Sarathy SM. PAH formation from jet stirred reactor pyrolysis of gasoline surrogates. Combustion and Flame 2020;219:312-26.
[24] FACE gasolines and blends with ethanol: Dethailed characterization of physical and chemical properties. CRC ed.; 2014.
[25] Sarathy SM, Farooq A, Kalghatgi GT. Recent progress in gasoline surrogate fuels. Progress in Energy and Combustion Science 2018;65:67-108.
[26] Huang C, Wei L, Yang B, Wang J, Li Y, Sheng L, et al. Lean premixed gasoline/oxygen flame studied with tunable synchrotron vacuum UV photoionization. Energy & Fuels 2006;20(4):1505-13.
[27] Li Y, Huang C, Wei L, Yang B, Wang J, Tian Z, et al. An experimental study of rich premixed gasoline/O2/Ar flame with tunable synchrotron vacuum ultraviolet photoionization. Energy & Fuels 2007;21(4):1931-41.
[28] Xu R, Saggese C, Lawson R, Movaghar A, Parise T, Shao J, et al. A physics-based approach to modeling real-fuel combustion chemistry – VI. Predictive kinetic models of gasoline fuels. Combustion and Flame 2020;220:475-87.
[29] Schlichting S, Zinsmeister J, Storch M, Mansbart M, Bauder U, Hall C, et al. BMWi project "Solare Kraftstoffe" - technical fuel assessment. 13th International colloquium fuels: Conventional and future energy for automobiles. Expert Verlag; 2021, p. 31-44.
[30] Zinsmeister J, Gaiser N, Melder J, Bierkandt T, Hemberger P, Kasper T, et al. On the diversity of fossil and alternative gasoline combustion chemistry: A comparative flow reactor study. Combustion and Flame 2022.
[31] Coryton. Certificate of Analysis, 2019.
[32] Pellegrin V. Molecular formulas of organic-compounds - the nitrogen rule and degree of unsaturation. Journal of Chemical Education 1983;60(8):626-33.
[33] Badertscher M, Bischofberger K, Munk ME, Pretsch E. A novel formalism to characterize the degree of unsaturation of organic molecules. J Chem Inf Comput Sci 2001;41(4):889-93.
[34] Yang B, Sun W, Moshammer K, Hansen N. Review of the influence of oxygenated additives on the combustion chemistry of hydrocarbons. Energy & Fuels 2021;35(17):13550-68.
[35] Ruwe L, Moshammer K, Hansen N, Kohse-Höinghaus K. Influences of the molecular fuel structure on combustion reactions towards soot precursors in selected alkane and alkene flames. Physical Chemistry Chemical Physics 2018;20(16):10780-95.
[36] Karavalakis G, Durbin TD, Yang J, Ventura L, Xu K. Fuel effects on PM emissions from different vehicle/engine configurations: A literature review. SAE Technical Paper 2018(2018-01-0349).
[37] Kohse-Höinghaus K, Oßwald P, Cool TA, Kasper T, Hansen N, Qi F, et al. Biofuel combustion chemistry: from ethanol to biodiesel. Angew Chem Int Ed Engl 2010;49(21):3572-97.

[38] Zhu R, Hu J, Bao X, He L, Zu L. Effects of aromatics, olefins and distillation temperatures (T50 & T90) on particle mass and number emissions from gasoline direct injection (GDI) vehicles. Energy Policy 2017;101:185-93.
[39] Yang JC, Roth P, Zhu HW, Durbin TD, Karavalakis G. Impacts of gasoline aromatic and ethanol levels on the emissions from GDI vehicles: Part 2. Influence on particulate matter, black carbon, and nanoparticle emissions. Fuel 2019;252:812-20.
[40] Yang JC, Roth P, Durbin T, Karavalakis G. Impacts of gasoline aromatic and ethanol levels on the emissions from GDI vehicles: Part 1. Influence on regulated and gaseous toxic pollutants. Fuel 2019;252:799-811.
[41] Singh R, Voice A, Fatouraie M, Levy R. Fuel effects on engine-out emissions Part 1 - comparing certification and market gasoline fuels. SAE International Journal of Advances and Current Practices in Mobility 2021;3(2021-01-0541):3121-37.
[42] Voice A, Singh R, Levy R, Fatouraie M. Fuel effects on engine-out emissions Part 2 - fuel properties correlations. SAE International Journal of Advances and Current Practices in Mobility 2021;3(2021-01-0538):3138-58.
[43] Chuahy FDF, Moses-DeBusk M, Curran SJ, Storey JME, Wagnon SW. The effects of distillation characteristics and aromatic content on low-load gasoline compression ignition (GCI) performance and soot emissions in a multi-cylinder engine. Fuel 2021;299.
[44] Oßwald P, Whitside R, Schäffer J, Köhler M. An experimental flow reactor study of the combustion kinetics of terpenoid jet fuel compounds: Farnesane, p-menthane and p-cymene. Fuel 2017;187:43-50.
[45] KG SHDBVC. Data set of 280 conventional Europe EN228 summer grade market gasolines (summer 2019) 2019.
[46] Kar K, Last T, Haywood C, Raine R. Measurement of vapor pressures and enthalpies of vaporization of gasoline and ethanol blends and their effects on mixture preparation in an SI engine. SAE International Journal of Fuels and Lubricants 2008;1(2008-01-0317):132-44.
[47] Balabin RM, Syunyaev RZ, Karpov SA. Molar enthalpy of vaporization of ethanol-gasoline mixtures and their colloid state. Fuel 2007;86(3):323-7.
[48] Linstrom P. NIST Chemistry WebBook, NIST Standard Reference Database 69; 2018. Available from: https://webbook.nist.gov/chemistry/.
[49] Chupka GM, Christensen E, Fouts L, Alleman TL, Ratcliff MA, McCormick RL. Heat of vaporization measurements for ethanol blends up to 50 volume percent in several hydrocarbon blendstocks and implications for knock in SI engines. SAE International Journal of Fuels and Lubricants 2015;8(2):251-63.
[50] Hunt RA. Relation of smoke point to molecular structure. Industrial and Engineering Chemistry 1953;45(3):602-6.
[51] Barrientos EJ, Anderson JE, Maricq MM, Boehman AL. Particulate matter indices using fuel smoke point for vehicle emissions with gasoline, ethanol blends, and butanol blends. Combustion and Flame 2016;167:308-19.
[52] Olson DB, Pickens JC, Gill RJ. The effects of molecular structure on soot formation II. Diffusion flames. Combustion and Flame 1985;62:43-60.
[53] Melder J, Zinsmeister J, Grein T, Jürgens S, Köhler M, Oßwald P. Comprehensive two-dimensional gas chromatography: a universal method for composition-based prediction of emission characteristics of complex fuels. submitted to Energy & Fuels.
[54] McEnally CS, Das DD, Pfefferle LD. Yield sooting index database volume 2: Sooting tendencies of a wide range of fuel compounds on a unified scale. V1. Harvard Dataverse; 2017.
[55] Richter S, Kathrotia T, Braun-Unkhoff M, Naumann C, Köhler M. Influence of oxymethylene ethers (OMEn) in mixtures with a Diesel surrogate. Energies 2021;14(23):7848.
[56] Richter S, Kathrotia T, Naumann C, Scheuermann S, Riedel U. Investigation of the sooting propensity of aviation fuel mixtures. CEAS Aeronautical Journal 2020;12(1):115-23.
[57] Köhler M, Oßwald P, Xu H, Kathrotia T, Hasse C, Riedel U. Speciation data for fuel-rich methane oxy-combustion and reforming under prototypical partial oxidation conditions. Chemical Engineering Science 2016;139:249-60.

[58] Kathrotia T, Naumann C, Oßwald P, Köhler M, Riedel U. Kinetics of ethylene glycol: The first validated reaction scheme and first measurements of ignition delay times and speciation data. Combustion and Flame 2017;179:172-84.
[59] Kathrotia T, Oßwald P, Köhler M, Slavinskaya N, Riedel U. Experimental and mechanistic investigation of benzene formation during atmospheric pressure flow reactor oxidation of n-hexane, n-nonane, and n-dodecane below 1200 K. Combustion and Flame 2018;194:426-38.
[60] Woortman DV, Jügens S, Untergehrer M, Rechenberger J, Fuchs M, Mehlmer N, et al. Greener aromatic antioxidants for aviation and beyond. Sustainable Energy & Fuels 2020;4(5):2153-63.
[61] Gaiser N, Bierkandt T, Oßwald P, Zinsmeister J, Kathrotia T, Shaqiri S, et al. Oxidation of oxymethylene ether (OME0−5): An experimental systematic study by mass spectrometry and photoelectron photoion coincidence spectroscopy. Fuel 2022;313:122650.
[62] Gaiser N, Zhang H, Bierkandt T, Schmitt S, Zinsmeister J, Kathrotia T, et al. Investigation of the combustion chemistry in laminar, low-pressure oxymethylene ether flames (OME0–4). Combustion and Flame 2022:112060.
[63] Köhler M, Kathrotia T, Oßwald P, Fischer-Tammer ML, Moshammer K, Riedel U. 1-, 2- and 3-Pentanol combustion in laminar hydrogen flames – a comparative experimental and modeling study. Combustion and Flame 2015;162(9):3197-209.
[64] Herrmann F, Jochim B, Oßwald P, Cai L, Pitsch H, Kohse-Höinghaus K. Experimental and numerical low-temperature oxidation study of ethanol and dimethyl ether. Combustion and Flame 2014;161(2):384-97.
[65] Oßwald P, Zinsmeister J, Kathrotia T, Alves-Fortunato M, Burger V, van der Westhuizen R, et al. Combustion kinetics of alternative jet fuels, Part-I: Experimental flow reactor study. Fuel 2021;302:120735.
[66] Kathrotia T, Oßwald P, Zinsmeister J, Methling T, Köhler M. Combustion kinetics of alternative jet fuels, Part-III: Fuel modeling and surrogate strategy. Fuel 2021;302:120737.
[67] Oßwald P, Köhler M. An atmospheric pressure high-temperature laminar flow reactor for investigation of combustion and related gas phase reaction systems. Rev Sci Instrum 2015;86(10):105109.
[68] Herrmann F, Oßwald P, Kohse-Höinghaus K. Mass spectrometric investigation of the low-temperature dimethyl ether oxidation in an atmospheric pressure laminar flow reactor. Proceedings of the Combustion Institute 2013;34(1):771-8.
[69] Biordi JC. Molecular beam mass spectrometry for studying the fundamental chemistry of flames. Progress in Energy and Combustion Science 1977;3:151-73.
[70] Beatrice C, Bertoli C, Del Biacomo N, Guido C, Migliaccio M. In-cylinder soot evolution analysis in a transparent research DI Diesel engine fed by oxygenated fuels. SAE Technical Paper 2002;2002-01-2851:147-60.
[71] Beatrice C, Di Blasio G, Guido C, Cannilla C, Bonura G, Frusteri F. Mixture of glycerol ethers as diesel bio-derivable oxy-fuel: Impact on combustion and emissions of an automotive engine combustion system. Applied Energy 2014;132:236-47.
[72] Chen LF, Stone R, Richardson D. A study of mixture preparation and PM emissions using a direct injection engine fuelled with stoichiometric gasoline/ethanol blends. Fuel 2012;96(1):120-30.
[73] Storch M, Hinrichsen F, Wensing M, Will S, Zigan L. The effect of ethanol blending on mixture formation, combustion and soot emission studied in an optical DISI engine. Applied Energy 2015;156:783-92.
[74] Yuan WH, Li YY, Dagaut P, Yang JZ, Qi F. Investigation on the pyrolysis and oxidation of toluene over a wide range conditions. I. Flow reactor pyrolysis and jet stirred reactor oxidation. Combustion and Flame 2015;162(1):3-21.
[75] Yuan WH, Li YY, Dagaut P, Yang JZ, Qi F. Investigation on the pyrolysis and oxidation of toluene over a wide range conditions. II. A comprehensive kinetic modeling study. Combustion and Flame 2015;162(1):22-40.
[76] Hansen N, Miller JA, Klippenstein SJ, Westmoreland PR, Kohse-Höinghaus K. Exploring formation pathways of aromatic compounds in laboratory-based model flames of aliphatic fuels. Combustion Explosion and Shock Waves 2012;48(5):508-15.

[77] Hansen N, Yang B, Braun-Unkhoff M, Ramirez A, Kukkadapu G. Molecular-growth pathways in premixed flames of benzene and toluene doped with propyne. Combustion and Flame 2022.
[78] Gail S, Dagaut P. Experimental kinetic study of the oxidation of p-xylene in a JSR and comprehensive detailed chemical kinetic modeling. Combustion and Flame 2005;141(3):281-97.
[79] Sun W, Hamadi A, Ardila FEC, Abid S, Chaumeix N, Comandini A. Insights into pyrolysis kinetics of xylene isomers behind reflected shock waves. Combustion and Flame 2022;244:112247.
[80] Cheng XG, Gao Z, Ren F, Rigopoulos S, Zhu L, Huang Z. Experimental and kinetic modeling study on sooting tendencies of alkylbenzene isomers. Fuel 2021;283.
[81] Weng JJ, Liu YX, Wang BY, Xing LL, Zhang LD, Tian ZY. Experimental and kinetic investigation of 1,2,4-trimethylbenzene oxidation at low temperature. Proceedings of the Combustion Institute 2017;36(1):909-17.